TABLE 1. Genetic alterations that collaborate in inducing acute leukemia according to "two-hit model"

Class I	Class II	Disease
FLT3 mutations	AML1 mutations	AML
FLT3 mutations	PML/RARα	AML:M3
FLT3-TKD	MLL-fusions	Pediatric ALL
Ras mutations	MLL-fusions	Pediatric ALL
Ras mutations	inv(16)	AML
c-Kit mutations	AML1/ETO	AML:M2(M1,4)
N-Ras mutations	AML1 mutations	MDS/AML
P53 mutations	MLL amplification	tMDS/AML
FLT3 mutations	NPM1 mutations	AML
(C/EBPα)	C/EBPα	AML

FLT3-TKD, FLT3 tyrosine kinase domain mutation. AML, acute myeloid leukemia. ALL, acute lymphoid leukemia. MDS/AML, myelodysplastic leukemia and subsequent AML. tMDS/AML, therapy-related MDS/AML.

et al., 1997; Fenske et al., 2004). So far, there have been only a few models of MDS that recapitulate the phenotype of human MDS; they include the *EVI1* BMT model (Buonamici et al., 2004), *NPM1* hetero mice (Grisendi et al., 2005; Sportoletti et al., 2008), and *NUP98/HOXD13* transgenic mice (Lin et al., 2005). We recently developed a novel mouse model of MDS using BMT of *AML1* mutants (Watanabe-Okochi et al., 2008). This review focuses on the pathology, latency to progression to leukemia, and biological characteristics of each MDS model, and discusses the usefulness of these models in developing new therapies for MDS.

EVI1 Overexpression in a Mouse BMT Model

The *MDS1–EVI1* gene (located on 3q26) encodes two distinct proteins, the MDS1-EVI1 and EVI1 zinc finger containing proteins, transcribed by different promoters (Fears et al., 1996; Buonamici et al., 2003). EVI1 lacks a PR domain that is contained in MDS-EVI1. EVI1 is transforming and can block hematopoietic differentiation of myeloid and erythroid lineages. Under physiological conditions, EVI1 is expressed only in immature hematopietic cells. Although recurrent chromosomal translocations are rare in MDS, the most frequent one is the inv(3)(q21q26), leading to inappropriate activation of the *EVI1* gene (Haase et al., 2007). In addition, EVI1 overexpression is observed in some AML (or MDS) cases without discernible chromosome abnormalities involving 3q26 (Russell et al., 1994; Zoccola et al., 2003). The t(3;21), fusing the N terminus of AML1 with nearly the entire portion of EVI1, is associated with aggressive transformation of MDS and the blast crisis of chronic myeloid leukemia (CML) (Maki et al., 2008).

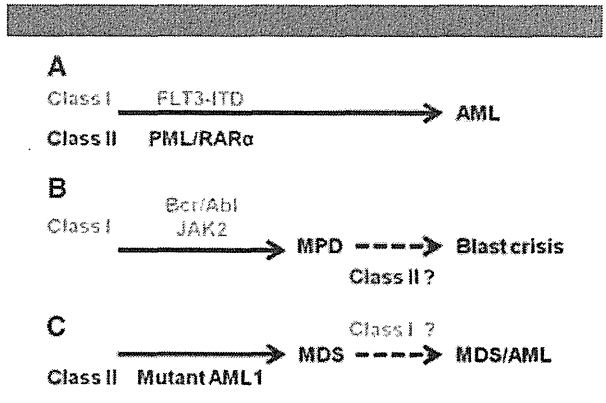

Fig. 1. Two-hit model of leukemogenesis. A: In some patients of AML, a FLT3-ITD mutation conferring growth advantage (class I) and a PML/RARα translocation abrogating myeloid differentiation are detected in combination. B: MPD caused by class I mutation may progress to blast crisis by a second hit of class II. C: In MDS caused by mutant AML1, dysplastic cells may acquire an additional hit of class I and transform into leukemia (MDS/AML). [Color figure can be viewed in the online issue, which is available at www.interscience.wiley.com.]

It was reported that overexpression of EVI1 in a mouse BMT model induced a fatal pancytopenia, characteristic of human MDS (Buonamici et al., 2004). Peripheral blood morphology remained normal for 7–8 months after BMT. However, EVI1-positive moribund mice revealed pancytopenia characterized by marked anisopoikilocytosis, increased numbers of polychromatophilic red blood cells (RBC), and the presence of Howell–Jolly bodies. Pancytopenia rapidly worsened, and the transplanted mice died 10–12 months after BMT. Spleen section revealed red pulp expansion, increased numbers of erythroid precursors, marked iron deposition, and apoptosis. A biopsy of the bone marrow demonstrated defective hematopoiesis characterized by erythroid and megakaryocytic hyperplasia and by dyserythropoiesis. However, the disease did not progress to acute myeloid leukemia. In vitro culture of lineage-negative bone marrow cells in the presence of erythropoietin revealed significantly decreased clonogenicity of EVI1-positive cells, whether they were from moribund mice, from mice 6 months before any hematologic abnormalities become apparent, or from freshly infected BM cells. In EVI1-positive moribund mice, quantitative RT-PCR of BM cells revealed downregulation of *EpoR* and *c-Mpl*, both important for terminal erythroid differentiation and platelet formation. However, why MDS cells with less clonogenic activities eventually dominate in the bone marrow to develop MDS remains totally elusive.

Although hyperproliferation, delayed differentiation, and impairment of erythroid differentiation occur immediately in the BM, it takes 10 months for the MDS phenotype to be evident in these mice, suggesting that MDS clones gradually dominate in the BM by unknown mechanisms. Alternatively, it is also possible that an additional hit is required for development of MDS. Since *EVI1* was retrovirally introduced, activation or inactivation of genes due to retroviral integration (insertional mutagenesis) might be a "second hit" (Slape et al., 2007).

Nucleophosmin1 (NPM1) Hetero Mice

Nucleophosmin1 (NPM1) is a nucleolar protein that has an important role in ribosome biogenesis. It also regulates the p53/ARF tumor suppressor pathway and plays a role in regulating centrosome duplication and genomic stability. The *NPM1* gene on 5q35 is frequently affected by chromosome translocation, mutation, and deletion in hematological disorders (Falini et al., 2005; Grisendi et al., 2006; Naoe et al., 2006). Deletion of chromosome 5 (5q or the whole chromosome) is observed in 30% of patients with MDS (Haase et al., 2007), and *NPM1-MLF1* translocation is recognized in AML/MDS (Grisendi et al., 2006; Naoe et al., 2006). In addition, mutations in NPM1 are frequently (approximately 35%) reported in AML, which cause mislocalization of NPM1 to the cytoplasm (Falini et al., 2005).

Although $NPM1^{-/-}$ mice were embryonically lethal between E11.5 and E12.5, $NPM1^{+/-}$ mice present features resembling human MDS at 6–18 months of age (Grisendi et al., 2005). The $NPM1^{+/-}$ mice had an increased MCV and anisocytosis of erythrocytes, without reticulocytosis, while RBC counts, hemoglobin levels, and serum levels of erythropoietin were all normal. In addition to the abnormalities in the erythroid lineage, some $NPM1^{+/-}$ mice had markedly elevated platelet counts.

Furthermore, MDS-like morphology was evident in the BM; 12 of 16 mice had erythroid dysplasia such as binucleated cells, abnormal mitosis, nuclear fragmentation, and irregular nuclear contour, and 7 of 11 had dysplastic megakaryocytes showing multiple separated nuclei, small oval nuclei in mature cytoplasm, and hypolobulated nuclei. Flow cytometry of BM cells revealed erythroid hyperplasia and increase of immature erythroblasts in these mice. After a 2-year follow-up, 12 out of 55 *NPM1*$^{+/-}$ mice (22%) developed transformed phenotypes; five MPD-like myeloid leukemia, four myeloid leukemia, two B-cell lymphoma and one T-cell lymphoma/leukemia, although whether MDS-like disease had preceded transformation was not mentioned. In contrast, *NPM1*$^{+/+}$ mice developed no hematological malignancy. Malignant cells retained the wild-type *NPM1* allele. These results demonstrate that NPM1 works as a haploinsufficient tumor suppressor of hematological malignancy. Thus, the *NPM1*$^{+/-}$ mouse is a reasonable model for MDS.

A NUP98/HOXD3 Transgenic Mouse Model

The *NUP98* gene, located on chromosome 11p15, encodes nucleoporin 98, a component of the nuclear pore complex involved in nucleo-cytoplasmic transport of mRNA and protein. In the chromosomes of AML, MDS, and CML cells, this gene frequently translocates to homeobox-containing (HOX) genes such as *HOXA9* and *HOXD13* (Romana et al., 2006; Slape et al., 2008a).

The *NUP98/HOXD13* fusion gene is generated by t(2;11) translocation, and the *NUP98/HOXD13* transgenic mice were reported to suffer from MDS-like disease (Lin et al., 2005). This was the first model that recapitulated all of the key features of MDS, including peripheral blood cytopenias, bone marrow dysplasia, and apoptosis, as well as transformation to AML. At 4–7 months of age, although apparently healthy, these mice showed an MDS-like phenotype characterized by anemia and leukopenia. Peripheral blood smear showed macrocytosis, polychromasia, anisocytosis, poikilocytosis, circulating nucleated RBC, giant platelets, and hypersegmented or hyposegmented granulocytes (including pseudo-Pelger–Huet anomaly). The bone marrow was normocellular to hypercellular with dysplasia and excessive apoptosis, which was compatible with the diagnostic criteria of human MDS. No mice lived beyond 14 months; by approximately 10 months, all of the mice had died of either leukemic transformation or severe anemia and leukopenia as a result of progressive MDS. It should be noted, however, that the BMT model of *NUP98/HOXD13* caused a different result (Pineault et al., 2003), where the recipient mice developed anemia and lymphopenia, and thereafter a minority of them developed MPD with increased neutrophil counts, but not MDS. Moreover, they did not progress to AML. One possible explanation for this discrepancy is the difference in the expression levels of the fusion gene product in these models.

The fact that AML occurs after a long latency in *NUP98/HOXD13* transgenic mice suggests additional mutations are required for progression to AML. Slape et al. (2007) reported the result of retroviral insertional mutagenesis used to identify genes that cooperate with *NUP98/HOXD13*. Among these genes are *Meis1*, *Mn1*, *Gata2*, *Erg*, and *Epor*. They also recently reported spontaneous mutations in *Nras*, *Kras*, and *Cbl* in acute nonlymphocytic leukemia in *NUP98/HOXD13* transgenic mice (Slape et al., 2008b). In BMT models, co-transduction of *NUP98/HOXD13* and wild-type *FLT3* or *Meis1*, a cofactor of HOX genes and inducer of FLT3, caused lethal AML to develop rapidly (Pineault et al., 2003; Palmqvist et al., 2006), presenting another example of "two-hit" leukemogenesis.

A BMT Model of AML1 with Point Mutations and Frameshift Mutations

The *AML1* (also known as *CBFα* or *Runx1*) gene is located on chromosome 21q22 and is the most frequent target of chromosomal translocation in leukemia. AML1 is indispensable for the establishment of definitive hematopoiesis (Okuda et al., 1996; Wang et al., 1996; Ichikawa et al., 2004). The *AML1* gene is also frequently mutated in AML M0, MDS/AML (MDS and subsequent AML), and therapy-related or radiation-related MDS (Osato, 2004). Although the vast majority of *AML1* mutations are located in the Runt homology domain (RHD), which mediates binding to DNA and core-binding factorβ (CBFβ), mutations in the C-terminal region outside the RHD have also been identified that were predominant in MDS/AML (Harada et al., 2004).

We recently established a mouse BMT model of MDS-RAEB and MDS/AML induced by *AML1* mutants found in patients with MDS and MDS/AML (Fig. 2) (Watanabe-Okochi et al., 2008). *AML1-D171N* has a point mutation in RHD, while *AML1-S291fsX300* has a frameshift mutation outside RHD that results in C-terminal truncation (hereafter referred to as D171N and S291fs, respectively). D171N lost its DNA-binding ability because of a point mutation in RHD essential for DNA binding, while S291fs had increased DNA-binding ability but lost transactivation potential because of a deletion in the C-terminal transactivation domain. Although both mutants work as dominant negative forms, the latter is more potent than the former (Harada et al., 2003, 2004). Follow-up of peripheral blood (PB) cell counts in recipients of both mutants revealed a gradual increase of GFP+ c-kit+ blasts over several months, especially in the D171N recipients. The smear specimens of PB showed that most recipients of each mutant suffered from multi-lineage dysplasia characteristic of MDS (Fig. 3). Erythroid dysplasia such as Howell–Jolly bodies, red cell polychromasia, and poikilocytosis were frequently detected. Most mice developed MDS and MDS/AML-like symptoms within 4–13 months after BMT, although the two mutants induced distinct phenotypes (Table 2). D171N recipients had hepatosplenomegaly and leukocytosis with marked myeloid dysplasia such as pseudo-Pelger–Huet anomaly and hypersegmented nuclei, and occasional giant platelets. On the other hand, S291fs recipients had pancytopenia with marked erythroid dysplasia such as increase of MCV, orthochromatic giant erythroblasts, and karyorrhexis, but less myeloid dysplasia. Interestingly, among retroviral integration sites identified, Evi1 seemed to collaborate with D171N, but not with S291fs, in inducing MDS/AML with an identical phenotype, B220+CD11b+. Collaboration between D171N and *Evi1* was confirmed by a BMT model, where coexpression of these genes induced acute leukemia of the same phenotype with much shorter latencies.

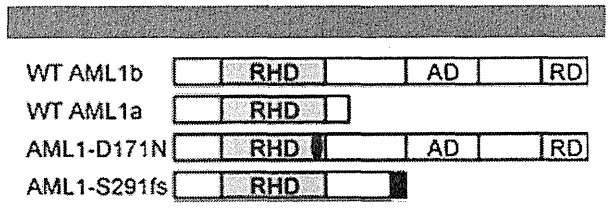

Fig. 2. Schemes of AML1 mutants. Wild-type AML1 has two isoforms, AML1a and AML1b. AML1-D171N mutant has a missense mutation in the Runt-homology domain that abrogates DNA-binding ability. AML1-S291fs has a frameshift mutation that results in C-terminal truncation. Both mutants have dominant-negative effects on wild-type AML1 (quoted and modified from Watanabe-Okochi et al., 2008).

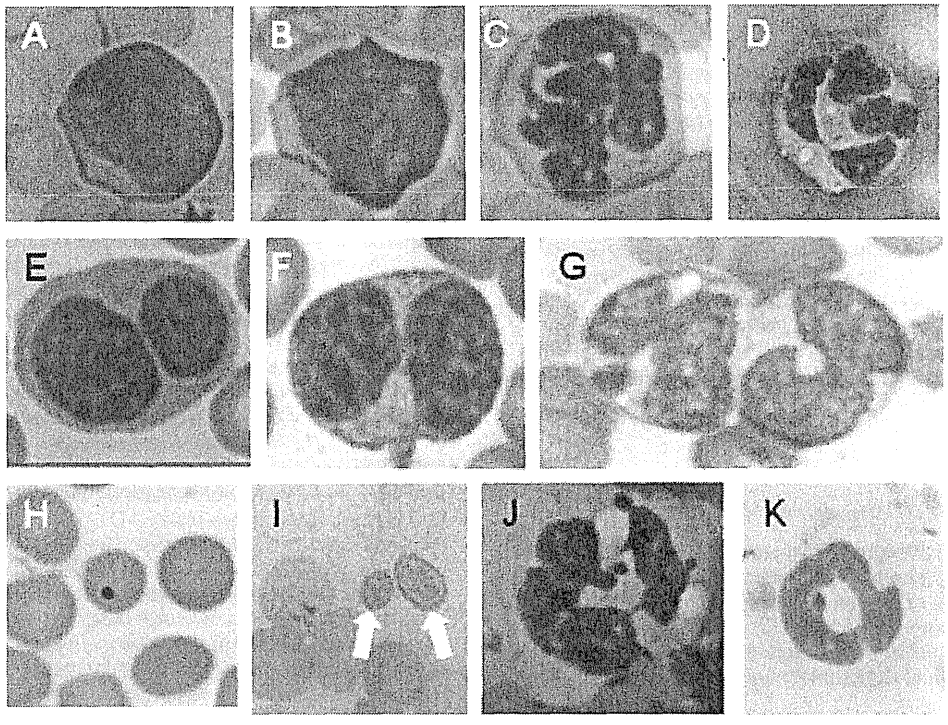

Fig. 3. Dysplastic features of MDS-like cells induced by mutant AML1. A and B: Myeloblasts; C and D: hypersegmented granulocyte; E and F: pseudo-Pelger–Huet anomaly; G: hyposegmented granulocytes; H: Howell–Jolly body in a red blood cell; I: giant platelet (white arrows); J and K: normal mouse granulocytes. All panels represent high-power 1000× magnification.

Our new MDS model has several advantages and implications over other models, as described below:

(1) Production of high-titer retroviruses and high expression levels in bone marrow cells can be efficiently achieved. The retrovirus vector pMYs is designed to achieve high expression in hematopoietic progenitor cells by featuring the MPSV-PCMV fusion LTR, and unlike other retrovirus vectors, retains splice donor and acceptor sites derived from the MFG vector to increase expression levels (Riviere et al., 1995; Kitamura et al., 2003). A packaging cell line, PlatE, enables high titers of retrovirus in combination with pMXs or pMYs vector (average: 10^7 infection U/mL) (Morita et al., 2000).
(2) Distinct types of mutations in the same gene caused different phenotypes. This emphasizes the importance of meticulous analysis of each mutation. In our models, the in vivo effects of each mutation can be tested more easily than in transgenic mice models.
(3) Our BMT model also provides a useful model for identification of "second hits" that play critical roles in leukemic transformation of MDS, which is known as "insertional mutagenesis of retroviruses" (Mucenski et al., 1988; Calmels et al., 2005; Yamashita et al., 2005; Jin et al., 2007; Slape et al., 2007).

TABLE 2. Two types of mutations in AML1 gene cause distinct phenotypes

	D171N (RHD mutant)	S291fs (frameshift and truncation)
c-kit+ blasts in PB	Gradual increase	Gradual increase
Overall survival	4–13 months	4–13 months
WBC at onset	Leukocytosis	Leukopenia
PB during follow-up	Multi-lineage dysplasia	Multi-lineage dysplasia
Erythroid dysplasia	Mild	Severe
Myeloid dysplasia	Severe	Mild
Platelet dysplasia	Giant platelet	None
Hepatosplenomegaly	Severe	Mild
Diagnosis		
MDS/AML	13/16	5/8
MDS-RAEB	2/16	2/8
de novo AML	1/16	0/8
Not determined	0/16	1/8
Retroviral integration into EVI1	7/15	0/8

WBC, white blood cells; PB, peripheral blood; RHD, Runt-homology domain.

Miscellaneous Models

Another example of an MDS model using homeobox genes (including *HOX* genes) are transgenic mice of *SALL4*, a zinc finger transcription factor and a homolog to *Drosophila spalt*. In humans, the SALL gene family (*SALL1-4*) is involved in normal development as well as in tumorigenesis. Ma et al. (2006) cloned *SALL4* and its isoforms (*SALL4A* and *SALL4B*), demonstrating that SALL4 was constitutively expressed in all AML samples examined. Interestingly, *SALL4B* transgenic mice presented MDS-like features at ages 6–8 months (penetrance: 100%). Some mice developed MDS as early as 2 months of age. Fifty percent of the mice with MDS symptoms subsequently progressed to transplantable AML (latency: 8–24 months). In vitro, both isoforms of SALL4 could bind β-catenin and activate the Wnt/β-catenin pathway, one of the plausible mechanisms of SALL4-induced leukemigenesis (Mikesch et al., 2007; Yang et al., 2008). At present, however, the clinical relationship between SALL4 and MDS is not clear.

Pauda et al. recently reported that overexpression of the activating mutant of Nras (NRASD12) and human BCL-2 (hBCL-2) in combination causes MDS and AML in mice (Omidvar et al., 2007). Both genes are prognostic features of MDS/AML. In the presence of NRASD12, expression of hBCL-2 by conditional mouse mammary tumor virus-long terminal repeat (MMTV-LTR) caused dysplastic features resembling human high-risk MDS, while its expression by myeloid MRP8 promoter caused AML. Of note, when hBCL-2 was switched off with doxycycline ("tet-off") in the MDS mice, a partial reversal of the phenotype was observed. These results indicate that BCL-2 expression is necessary for both initiating this neoplasm and for (irreversible) fatal disease progression. This progression was accompanied by an increase in reactive oxygen species (ROS), which led to increased double-strand breaks of DNA and inaccurate repair by the error-prone nonhomologous end-joining pathway (Rassool et al., 2007).

Transforming growth factor-β (TGF-β) is a myelosuppressive cytokine that has been implicated in the hematopoietic suppression of MDS. Zhou et al. (2008) demonstrated that the TGF-β pathway was activated in all MDS patients examined. Transgenic mice expressed a fusion gene of albumin and TGF-β1 (Alb-TGF-β1) consisting of modified porcine TGF-β1 cDNA under the control of the regulatory elements of the mouse albumin gene, becoming anemic at 3 weeks. Histological examination of their BM revealed dysplastic megakaryocytes and focal marrow reticulin fibrosis, features that resemble human BM failure states such as MDS (Sanderson et al., 1995; Zhou et al., 2008). Progression to AML was not observed. Inhibition of the TGF-β pathway with a small molecule inhibitor of TGF-βreceptor I kinase (TBRI), SD-208, improved anemia and the colony-forming ability of erythroid and myeloid lineages in Alb-TGF-β transgenic mice.

In addition to mouse MDS models, a mouse xenograft model has become available to directly analyze human MDS cells in vivo. Traditional nonobese diabetic-severe combined immunodeficient (NOD/SCID) mice or NOD/SCID common γ chain deficient (NOG) mice are usually used for the engraftment of human cells, including leukemic cells. NOD/SCID-β2m$^{-/-}$ mice lack natural killer (NK) cell activity in addition to T and B cells and were therefore expected to be a better recipient of human cells as a xenograft model. However, this model did not support the engraftment of human MDS cells. Thanopoulou et al. (2004) genetically engineered NOD/SCID-β2m$^{-/-}$ mice to produce human interleukin-3 (IL-3), granulocyte-macrophage colony-stimulating factor (GM-CSF), and Steel factor (SF) (NOD/SCID-β2m$^{-/-}$-3/GM/SF mice), which enabled engraftment of human MDS cells in mice. This also indicates that MDS cells are factor dependent in vivo and require additional mutations for leukemic transformation.

Conclusions and Perspectives

Because MDS is a heterologous disease, it has been difficult to model all of the features of MDS in a single mouse model. However, we now have available at least three animal models that recapitulate human MDS with progression to AML (*NPM1*$^{+/-}$ mice, *NUP98/HOXD13* mice, and BMT models of mutant *AML1*). Intriguingly, Chung et al. (2008) have demonstrated that *NUP98/HOXD13*-induced MDS is transplantable, and progression to AML was observed in secondary recipients. They identified MDS-initiating cells (M-IC) with long-term repopulating capacity. Further analysis of MDS biology and evaluation of MDS therapy using various animal models will open the door to complete control of this intractable disease.

Literature Cited

Bacher U, Haferlach T, Schoch C, Kern W, Schnittger S. 2006. Implications of NRAS mutations in AML: a study of 2502 patients. Blood 107:3847–3853.

Buonamici S, Chakraborty S, Senyuk V, Nucifora G. 2003. The role of EVI1 in normal and leukemic cells. Blood Cells Mol Dis 31:206–212.

Buonamici S, Li D, Chi Y, Zhao R, Wang X, Brace L, Ni H, Saunthararajah Y, Nucifora G. 2004. EVI1 induces myelodysplastic syndrome in mice. J Clin Invest 114:713–719.

Calmels B, Ferguson C, Laukkanen MO, Adler R, Faulhaber M, Kim HJ, Sellers S, Hematti P, Schmidt M, von Kalle C, Akagi K, Donahue RE, Dunbar CE. 2005. Recurrent retroviral vector integration at the Mds1/Evi1 locus in nonhuman primate hematopoietic cells. Blood 106:2530–2533.

Chung YJ, Choi CW, Slape C, Fry T, Aplan PD. 2008. Transplantation of a myelodysplastic syndrome by a long-term repopulating hematopoietic cell. Proc Natl Acad Sci 105:14088–14093.

Falini B, Mecucci C, Tiacci E, Alcalay M, Rosati R, Pasqualucci L, La Starza R, Diverio D, Colombo E, Santucci A, Bigerna B, Pacini R, Pucciarini A, Liso A, Vignetti M, Fazi P, Meani N, Pettirossi V, Saglio G, Mandelli F, Lo-Coco F, Pelicci PG, Martelli MF. 2005. Cytoplasmic nucleophosmin in acute myelogenous leukemia with a normal karyotype. N Engl J Med 352:254–266.

Fears S, Mathieu C, Zeleznik-Le N, Huang S, Rowley JD, Nucifora G. 1996. Intergenic splicing of MDS1 and EVI1 occurs in normal tissues as well as in myeloid leukemia and produces a new member of the PR domain family. Proc Natl Acad Sci USA 93:1642–1647.

Fenske TS, Pengue G, Mathews V, Hanson PT, Hamm SE, Riaz N, Graubert TA. 2004. Stem cell expression of the AML1/ETO fusion protein induces a myeloproliferative disorder in mice. Proc Natl Acad Sci USA 101:15184–15189.

Gilliland DG. 2001. Hematologic malignancies. Curr Opin Hematol 8:189–191.

Gilliland DG, Griffin JD. 2002. The roles of FLT3 in hematopoiesis and leukemia. Blood 100:1532–1542.

Grisendi S, Bernardi R, Rossi M, Cheng K, Khandker L, Manova K, Pandolfi PP. 2005. Role of nucleophosmin in embryonic development and tumorigenesis. Nature 437:147–153.

Grisendi S, Mecucci C, Falini B, Pandolfi PP. 2006. Nucleophosmin and cancer. Nat Rev Cancer 6:493–505.

Grisolano JL, Wesselschmidt RL, Pelicci PG, Ley TJ. 1997. Altered myeloid development and acute leukemia in transgenic mice expressing PML-RAR alpha under control of cathepsin G regulatory sequences. Blood 89:376–387.

Haase D, Germing U, Schanz J, Pfeilstocker M, Nosslinger T, Hildebrandt B, Kundgen A, Lubbert M, Kunzmann R, Giagounidis AA, Aul C, Trumper L, Krieger O, Stauder R, Muller TH, Wimazal F, Valent P, Fonatsch C, Steidl C. 2007. New insights into the prognostic impact of the karyotype in MDS and correlation with subtypes: evidence from a core dataset of 2124 patients. Blood 110:4385–4395.

Harada H, Harada Y, Tanaka H, Kimura A, Inaba T. 2003. Implications of somatic mutations in the AML1 gene in radiation-associated and therapy-related myelodysplastic syndrome/acute myeloid leukemia. Blood 101:673–680.

Harada H, Harada Y, Niimi H, Kyo T, Kimura A, Inaba T. 2004. High incidence of somatic mutations in the AML1/RUNX1 gene in myelodysplastic syndrome and low blast percentage myeloid leukemia with myelodysplasia. Blood 103:2316–2324.

Ichikawa M, Asai T, Saito T, Seo S, Yamazaki I, Yamagata T, Mitani K, Chiba S, Ogawa S, Kurokawa M, Hirai H. 2004. AML-1 is required for megakaryocytic maturation and lymphocytic differentiation, but not for maintenance of hematopoietic stem cells in adult hematopoiesis. Nat Med 10:299–304.

Jin G, Yamazaki Y, Takuwa M, Takahara T, Kaneko K, Kuwata T, Miyata S, Nakamura T. 2007. Trib1 and Evi1 cooperate with Hoxa and Meis1 in myeloid leukemogenesis. Blood 109:3998–4005.

Kelly LM, Kutok JL, Williams IR, Boulton CL, Amaral SM, Curley DP, Ley TJ, Gilliland DG. 2002. PML/RARalpha and FLT3-ITD induce an APL-like disease in a mouse model. Proc Natl Acad Sci USA 99:8283–8288.

Kirstetter P, Schuster MB, Bereshchenko O, Moore S, Dvinge H, Kurz E, Theilgaard-Monch K, Mansson R, Pedersen TA, Pabst T, Schrock E, Porse BT, Jacobsen SE, Bertone P, Tenen DG, Nerlov C. 2008. Modeling of C/EBPalpha mutant acute myeloid leukemia reveals a common expression signature of committed myeloid leukemia-initiating cells. Cancer Cell 13:299–310.

Kitamura T, Koshino Y, Shibata F, Oki T, Nakajima H, Nosaka T, Kumagai H. 2003. Retrovirus-mediated gene transfer and expression cloning: powerful tools in functional genomics. Exp Hematol 31:1007–1014.

Kiyoi H, Naoe T, Yokota S, Nakao M, Minami S, Kuriyama K, Takeshita A, Saito K, Hasegawa S, Shimodaira S, Tamura J, Shimazaki C, Matsue K, Kobayashi H, Arima N, Suzuki R, Morishita H, Saito H, Ueda R, Ohno R. 1997. Internal tandem duplication of FLT3 associated with leukocytosis in acute promyelocytic leukemia. Leukemia Study Group of the Ministry of Health and Welfare (Kohseisho). Leukemia 11:1447–1452.

Kottaridis PD, Gale RE, Frew ME, Harrison G, Langabeer SE, Belton AA, Walker H, Wheatley K, Bowen DT, Burnett AK, Goldstone AH, Linch DC. 2001. The presence of a FLT3 internal tandem duplication in patients with acute myeloid leukemia (AML) adds important prognostic information to cytogenetic risk group and response to the first cycle of chemotherapy: analysis of 854 patients from the United Kingdom Medical Research Council AML 10 and 12 trials. Blood 98:1752–1759.

Lin YW, Slape C, Zhang Z, Aplan PD. 2005. NUP98-HOXD13 transgenic mice develop a highly penetrant, severe myelodysplastic syndrome that progresses to acute leukemia. Blood 106:287–295.

Ma Y, Cui W, Yang J, Qu J, Di C, Amin HM, Lai R, Ritz J, Krause DS, Chai L. 2006. SALL4, a novel oncogene, is constitutively expressed in human acute myeloid leukemia (AML) and induces AML in transgenic mice. Blood 108:2726–2735.

Maki K, Yamagata T, Mitani K. 2008. Role of the RUNX1-EVI1 fusion gene in leukemogenesis. Cancer Sci 99:1878–1883.

Malcovati L, Nimer SD. 2008. Myelodysplastic syndromes: diagnosis and staging. Cancer Control 15:4–13.

Mikesch JH, Steffen B, Berdel WE, Serve H, Muller-Tidow C. 2007. The emerging role of Wnt signaling in the pathogenesis of acute myeloid leukemia. Leukemia 21:1638–1647.

Morita S, Kojima T, Kitamura T. 2000. Plat-E: an efficient and stable system for transient packaging of retroviruses. Gene Ther 7:1063–1066.

Mucenski ML, Taylor BA, Ihle JN, Hartley JW, Morse HC 3rd, Jenkins NA, Copeland NG. 1988. Identification of a common ecotropic viral integration site, Evi-1, in the DNA of AKXD murine myeloid tumors. Mol Cell Biol 8:301–308.

Muller AM, Duque J, Shizuru JA, Lubbert M. 2008. Complementing mutations in core binding factor leukemias: from mouse models to clinical applications. Oncogene 27:5759–5773.

Naoe T, Suzuki T, Kiyoi H, Urano T. 2006. Nucleophosmin: a versatile molecule associated with hematological malignancies. Cancer Sci 97:963–969.

Nerlov C. 2004. C/EBPalpha mutations in acute myeloid leukaemias. Nat Rev Cancer 4:394–400.

Okuda T, van Deursen J, Hiebert SW, Grosveld G, Downing JR. 1996. AML1, the target of multiple chromosomal translocations in human leukemia, is essential for normal fetal liver hematopoiesis. Cell 84:321–330.

Omidvar N, Kogan S, Beurlet S, le Pogam C, Janin A, West R, Noguera ME, Reboul M, Soulie A, Leboeuf C, Setterblad N, Felsher D, Lagasse E, Mohamedali A, Thomas NS, Fenaux P, Fontenay M, Pla M, Mufti GJ, Weissman I, Chomienne C, Padua RA. 2007. BCL-2 and mutant NRAS interact physically and functionally in a mouse model of progressive myelodysplasia. Cancer Res 67:11657–11667.

Ono R, Nakajima H, Ozaki K, Kumagai H, Kawashima T, Taki T, Kitamura T, Hayashi Y, Nosaka T. 2005. Dimerization of MLL fusion proteins and FLT3 activation synergize to induce multiple-lineage leukemogenesis. J Clin Invest 115:919–929.

Osato M. 2004. Point mutations in the RUNX1/AML1 gene: another actor in RUNX leukemia. Oncogene 23:4284–4296.

Palmqvist L, Argiropoulos B, Pineault N, Abramovich C, Sly LM, Krystal G, Wan A, Humphries RK. 2006. The Flt3 receptor tyrosine kinase collaborates with NUP98-HOX fusions in acute myeloid leukemia. Blood 108:1030–1036.

Pineault N, Buske C, Feuring-Buske M, Abramovich C, Rosten P, Hogge DE, Aplan PD, Humphries RK. 2003. Induction of acute myeloid leukemia in mice by the human leukemia-specific fusion gene NUP98-HOXD13 in concert with Meis1. Blood 101:4529–4538.

Pollock JL, Westervelt P, Kurichety AK, Pelicci PG, Grisolano JL, Ley TJ. 1999. A bcr-3 isoform of RARalpha-PML potentiates the development of PML-RARalpha-driven acute promyelocytic leukemia. Proc Natl Acad Sci USA 96:15103–15108.

Rassool FV, Gaymes TJ, Omidvar N, Brady N, Beurlet S, Pla M, Reboul M, Lea N, Chomienne C, Thomas NS, Mufti GJ, Padua RA. 2007. Reactive oxygen species, DNA damage, and error-prone repair: a model for genomic instability with progression in myeloid leukemia? Cancer Res 67:8762–8771.

Riviere I, Brose K, Mulligan RC. 1995. Effects of retroviral vector design on expression of human adenosine deaminase in murine bone marrow transplant recipients engrafted with genetically modified cells. Proc Natl Acad Sci USA 92:6733–6737.

Romana SP, Radford-Weiss I, Ben Abdelali R, Schluth C, Petit A, Dastugue N, Talmant P, Bilhou-Nabera C, Mugneret F, Lafage-Pochitaloff M, Mozziconacci MJ, Andrieu J, Lai JL, Terre C, Rack K, Cornillet-Lefebvre P, Luquet I, Nadal N, Nguyen-Khac F, Perot C, Van den Akker J, Fert-Ferrer S, Cabrol C, Charrin C, Tigaud I, Poirel H, Vekemans M, Bernard OA, Berger R. 2006. NUP98 rearrangements in hematopoietic malignancies: a study of the Groupe Francophone de Cytogenetique Hematologique. Leukemia 20:696–706.

Russell M, List A, Greenberg P, Woodward S, Glinsmann B, Parganas E, Ihle J, Taetle R. 1994. Expression of EVI1 in myelodysplastic syndromes and other hematologic malignancies without 3q26 translocations. Blood 84:1243–1248.

Sanderson N, Factor V, Nagy P, Kopp J, Kondaiah P, Wakefield L, Roberts AB, Sporn MB, Thorgeirsson SS. 1995. Hepatic expression of mature transforming growth factor beta 1 in transgenic mice results in multiple tissue lesions. Proc Natl Acad Sci USA 92:2572–2576.

Schessl C, Rawat VP, Cusan M, Deshpande A, Kohl TM, Rosten PM, Spiekermann K, Humphries RK, Schnittger S, Kern W, Hiddemann W, Quintanilla-Martinez L, Bohlander SK, Feuring-Buske M, Buske C. 2005. The AML1-ETO fusion gene and the FLT3 length mutation collaborate in inducing acute leukemia in mice. J Clin Invest 115:2159–2168.

Slape C, Hartung H, Lin YW, Bies J, Wolff L, Aplan PD. 2007. Retroviral insertional mutagenesis identifies genes that collaborate with NUP98-HOXD13 during leukemic transformation. Cancer Res 67:5148–5155.

Slape C, Lin YW, Hartung H, Zhang Z, Wolff L, Aplan PD. 2008a. NUP98-HOX translocations lead to myelodysplastic syndrome in mice and men. J Natl Cancer Inst Monogr 2008: 64–68.

Slape C, Liu LY, Beachy S, Aplan PD. 2008b. Leukemic transformation in mice expressing a NUP98-HOXD13 transgene is accompanied by spontaneous mutations in Nras, Kras, and Cbl. Blood 112:2017–2019.

Sportoletti P, Grisendi S, Majid SM, Cheng K, Clohessy JG, Viale A, Teruya-Feldstein J, Pandolfi PP. 2008. Npm1 is a haploinsufficient suppressor of myeloid and lymphoid malignancies in the mouse. Blood 111:3859–3862.

Thanopoulou E, Cashman J, Kakagianne T, Eaves A, Zoumbos N, Eaves C. 2004. Engraftment of NOD/SCID-beta2 microglobulin null mice with multilineage neoplastic cells from patients with myelodysplastic syndrome. Blood 103:4285–4293.

Thiede C, Steudel C, Mohr B, Schaich M, Schakel U, Platzbecker U, Wermke M, Bornhauser M, Ritter M, Neubauer A, Ehninger G, Illmer T. 2002. Analysis of FLT3-activating mutations in 979 patients with acute myelogenous leukemia: association with FAB subtypes and identification of subgroups with poor prognosis. Blood 99:4326–4335.

Wang Q, Stacy T, Binder M, Marin-Padilla M, Sharpe AH, Speck NA. 1996. Disruption of the Cbfa2 gene causes necrosis and hemorrhaging in the central nervous system and blocks definitive hematopoiesis. Proc Natl Acad Sci USA 93:3444–3449.

Watanabe-Okochi N, Kitaura J, Ono R, Harada H, Harada Y, Komeno Y, Nakajima H, Nosaka T, Inaba T, Kitamura T. 2008. AML1 mutations induced MDS and MDS/AML in a mouse BMT model. Blood 111:4297–4308.

Yamashita N, Osato M, Huang L, Yanagida M, Kogan SC, Iwasaki M, Nakamura T, Shigesada K, Asou N, Ito Y. 2005. Haploinsufficiency of Runx1/AML1 promotes myeloid features and leukaemogenesis in BXH2 mice. Br J Haematol 131:495–507.

Yan M, Kanbe E, Peterson LF, Boyapati A, Miao Y, Wang Y, Chen IM, Chen Z, Rowley JD, Willman CL, Zhang DE. 2006. A previously unidentified alternatively spliced isoform of t(8;21) transcript promotes leukemogenesis. Nat Med 12:945–949.

Yan M, Ahn EY, Hiebert SW, Zhang DE. 2008. RUNX1/AML1 DNA binding domain and ETO/MTG8 NHR2 dimerization domain are critical to AML1-ETO9a leukemogenesis. Blood 113:883–886.

Yang J, Chai L, Gao C, Fowles TC, Alipio Z, Dang H, Xu D, Fink LM, Ward DC, Ma Y. 2008. SALL4 is a key regulator of survival and apoptosis in human leukemic cells. Blood 112:805–813.

Zhou L, Nguyen AN, Sohal D, Ying Ma J, Pahanish P, Gundabolu K, Hayman J, Chubak A, Mo Y, Bhagat TD, Das B, Kapoun AM, Navas TA, Parmar S, Kambhampati S, Pellagatti A, Braunchweig I, Zhang Y, Wickrema A, Medicherla S, Boultwood J, Platanias LC, Higgins LS, List AF, Bitzer M, Verma A. 2008. Inhibition of the TGF-beta receptor I kinase promotes hematopoiesis in MDS. Blood 112:3434–3443.

Zoccola D, Legros L, Cassuto P, Fuzibet JG, Nucifora G, Raynaud SD. 2003. A discriminating screening is necessary to ascertain EVI1 expression by RT-PCR in malignant cells from the myeloid lineage without 3q26 rearrangement. Leukemia 17:643–645.

MOLECULAR AND CELLULAR BIOLOGY, Apr. 2009, p. 1796–1813 Vol. 29, No. 7
0270-7306/09/$08.00+0 doi:10.1128/MCB.01423-08

A Rac GTPase-Activating Protein, MgcRacGAP, Is a Nuclear Localizing Signal-Containing Nuclear Chaperone in the Activation of STAT Transcription Factors▽†

Toshiyuki Kawashima,[1]‡* Ying Chun Bao,[1]‡ Yukinori Minoshima,[1] Yasushi Nomura,[1] Tomonori Hatori,[1] Tetsuya Hori,[2] Tatsuo Fukagawa,[2] Toshiyuki Fukada,[3,4] Noriko Takahashi,[1] Tetsuya Nosaka,[1,5] Makoto Inoue,[6] Tomohiro Sato,[6,7] Mutsuko Kukimoto-Niino,[6] Mikako Shirouzu,[6] Shigeyuki Yokoyama,[6,7] and Toshio Kitamura[1]*

Division of Cellular Therapy, Institute of Medical Science, University of Tokyo, Minato-ku, Tokyo 108-8639, Japan[1]; Department of Molecular Genetics, National Institute of Genetics and the Graduate University for Advanced Studies, Mishima, Shizuoka 411-8540, Japan[2]; Laboratory for Cytokine Signaling, RIKEN Research Center for Allergy and Immunology,[3] and Protein Research Group, Genomic Sciences Center, Yokohama Institute, RIKEN,[6] 1-7-22 Suehiro-cho, Tsurumi, Yokohama 230-0045, Japan; Department of Allergy and Immunology, Osaka University Graduate School of Medicine, Osaka University, 2-2 Yamada-oka, Suita, Osaka 565-0871, Japan[4]; Department of Microbiology, Mie University Graduate School of Medicine, 2-174 Edobashi, Tsu 514-8507, Japan[5]; and Department of Biophysics and Biochemistry, Graduate School of Science, University of Tokyo, 7-3-1 Hongo, Bunkyo-ku, Tokyo 113-0033, Japan[7]

Received 10 September 2008/Returned for modification 1 November 2008/Accepted 12 January 2009

In addition to their pleiotropic functions under physiological conditions, transcription factors STAT3 and STAT5 also have oncogenic activities, but how activated STATs are transported to the nucleus has not been fully understood. Here we show that an MgcRacGAP mutant lacking its nuclear localizing signal (NLS) blocks nuclear translocation of p-STATs both in vitro and in vivo. Unlike wild-type MgcRacGAP, this mutant did not promote complex formation of phosphorylated STATs (p-STATs) with importin α in the presence of GTP-bound Rac1, suggesting that MgcRacGAP functions as an NLS-containing nuclear chaperone. We also demonstrate that mutants of STATs lacking the MgcRacGAP binding site (the strand βb) are hardly tyrosine phosphorylated after cytokine stimulation. Intriguingly, mutants harboring small deletions in the C′-adjacent region (βb-βc loop region) of the strand βb became constitutively active with the enhanced binding to MgcRacGAP. The molecular basis of this phenomenon will be discussed, based on the computer-assisted tertiary structure models of STAT3. Thus, MgcRacGAP functions as both a critical mediator of STAT's tyrosine phosphorylation and an NLS-containing nuclear chaperone of p-STATs.

The STAT (signal transducers and activators of transcription) family proteins (STAT1 to -4, -5A, -5B, and -6) are phosphorylated by cytokine stimulation, form homo- or heterodimers, and enter the nucleus, where they regulate expression of their target genes (6, 13). STATs have a variety of functions, including antiapoptosis, proliferation, differentiation, inflammation, and development under physiological conditions, and of note, the oncogenic activities of STAT3 and STAT5 have also been demonstrated under pathological conditions (5).

A small GTPase Rac1 is implicated in cytoskeletal organization, membrane ruffling, production of superoxide, phagocytosis, and chemotaxis as well as regulation of the cell cycle (15, 39). Recent studies revealed its distinct roles in nuclear translocation of phosphorylated STATs (p-STATs) and β-catenin and also its nuclear accumulation in the G_2 phase, promoting cell division (17, 31, 47). MgcRacGAP is an evolutionarily conserved GTPase-activating protein (GAP) for Rho family GTPases. We and others previously showed that MgcRacGAP controls the mitotic spindle through associating α-, β-, and γ-tubulin, Rho family GTPases, and a kinesin protein, MKLP1, and plays essential roles in the completion of cytokinesis, accumulating to the midbody (12, 16, 32). Very recently, Yamada et al. reported that conditional knockout of MgcRacGAP results in acute apoptosis even before the failure of cytokinesis in interleukin-7 (IL-7)-expanded $B220^+$ cells (48), indicating that MgcRacGAP is not simply involved in cell division but also in cell survival, at least in IL-7-expanded $B220^+$ cells.

Molecular trafficking between the nucleus and cytoplasm occurs via nuclear pore complexes. To enter the nucleus, nuclear proteins larger than ~50 kDa usually harbor a functional nuclear localization signal (NLS) or bind NLS-containing chaperones. The best-characterized NLS is the mono- or bipartite polybasic NLS. Polybasic NLS-containing proteins are usually recognized by importin α/β heterodimers, importin β docks the ternary complex to the nuclear pore, and the complex migrates into the nucleus. Then, the GTP-bound form of small GTPase Ran directly binds to importin β in the complex,

* Corresponding author. Mailing address: Division of Cellular Therapy, Institute of Medical Science, University of Tokyo, Minato-ku, Tokyo 108-8639, Japan. Phone: 81-3-5449-5758. Fax: 81-3-5449-5453. E-mail for Toshiyuki Kawashima: kkawa@ims.u-tokyo.ac.jp. E-mail for Toshio Kitamura: kitamura@ims.u-tokyo.ac.jp.

† Supplemental material for this article may be found at http://mcb.asm.org/.

‡ T.K. and Y.C.B. contributed equally to this work.

▽ Published ahead of print on 21 January 2009.

followed by disassembly of the complex inside the nucleus (11, 29). In addition to the polybasic NLS proline, tyrosine-containing NLSs (PY-NLSs) have been reported to be a different class of NLS; these NLSs mediate direct binding of NLS-containing proteins to karyopherin β2 (24).

How activated STATs are transported to the nucleus has been investigated; activated STAT1 and STAT3 were reported to bind importin α5 and several importin αs, respectively, which mediated the nuclear transport of STATs (25, 26, 30, 42, 44). Molecules other than importins and Ran also participate in the regulation of the nuclear translocation of STATs (27). We recently found that GTP-bound Rac1 and MgcRacGAP form a ternary complex with p-STATs and play critical roles in the nuclear translocation of p-STATs via the importin α/β pathway in an in vitro nuclear transport assay (17). However, it remained elusive how GTP-bound Rac1 and MgcRacGAP mediate the complex formation of p-STATs with importin αs. Moreover, the regulation of nuclear import of activated STATs by MgcRacGAP has not been fully demonstrated in vivo, because MgcRacGAP also plays an essential role in the completion of cytokinesis (12, 16, 33, 45). Therefore, the phenotypes observed in MgcRacGAP-depleted cells may include the effects of cytokinesis failure.

In the present work, we demonstrate that the NLS of MgcRacGAP plays essential roles in the nuclear import of p-STATs not only in vitro but also in vivo, by using MgcRacGAP conditional knockout DT40 cells expressing MgcRacGAP mutants lacking the NLS. We also found that the STAT mutants that did not bind MgcRacGAP were hardly phosphorylated on their tyrosine residues by cytokine stimulation, while the STAT mutants that preferentially bound MgcRacGAP exerted strong transcriptional activities even without cytokine stimulation. Thus, MgcRacGAP accompanied by GTP-bound Rac1 is not only an NLS-containing nuclear chaperone of p-STATs but also a critical activator of STAT proteins.

MATERIALS AND METHODS

Purification of recombinant proteins in Sf-9 cells. Purification of recombinant proteins using Sf-9 cells was done as described previously (17). To confirm the purity, the eluted proteins were subjected to sodium dodecyl sulfate-polyacrylamide gel electrophoresis (SDS-PAGE), followed by Coomassie blue (CBB) staining or by Western blotting. Purified His-tagged L69Ran and His-tagged N24Ran were purchased from Cytoskeleton, Inc.

Import assays with permeabilized cells. HeLa cells were grown on poly(L-lysine)-coated coverslips and permeabilized with 40 μg/ml digitonin (Roche) in transport buffer (TB; 20 mM HEPES, pH 7.3, 110 mM KO-acetate, 2 mM $Mg(O\text{-acetate})_2$, 1 mM EGTA, 2 mM dithiothreitol, 0.4 mM phenylmethylsulfonyl fluoride, 3 μg/ml of aprotinin, 2 μg/ml of pepstatin A, 1 μg/ml of leupeptin, 20 mg/ml of bovine serum albumin) for 10 min at room temperature. Subsequently, the cells were washed twice in TB to wash out cytoplasmic proteins. Incubation with 50 μl import mix (IM) was performed at 37°C for 30 min. The IM contained TB, an energy-regenerating system (ERS; 0.5 mM ATP, 0.5 mM GTP, 10 mM creatine phosphate, 30 U/ml creatine phosphokinase) and combinations of 1 μM of the purified proteins indicated in Fig. 2B, below (see also Fig. S2 and S3 in the supplemental material). Following the import reaction, the cells were washed with ice-cold TB and immunostained.

Immunostaining and antibodies. HeLa cells were immunostained as described previously (12). Rabbit anti-STAT5A, anti-STAT3, antihemagglutinin, anti-NF-κB p65, goat anti-glutathione *S*-transferase (anti-GST) (Santa Cruz), mouse anti-Flag (M2; Sigma), rabbit anti-Flag (Zymed), and affinity-purified rabbit anti-MgcRasGAP (12) antibodies (Abs) were used for the first Ab. For the secondary Ab and DNA staining, fluorescein isothiocyanate- or rhodamine-conjugated goat anti-rabbit immunoglobulin (Ig; Wako), fluorescein isothiocyanate- or rhodamine-conjugated goat anti-mouse Ig (Sigma), or rhodamine-conjugated anti-goat Ig (Wako) and 4′,6-diamino-2-phenylindole (DAPI) were used.

Microscopy. Fixed fluorescence images were analyzed on a confocal microscope (FLUOVIEW FV300 scanning laser biological microscope IX70 system; Olympus). Living cells expressing green fluorescent protein (GFP)-fusion proteins were viewed with a fluorescence microscope IX70 (Olympus) equipped with a SenSys/OL cold charge-coupled-device camera (Olympus).

In vitro binding assay, immunoprecipitation, and Western blotting. Immunoprecipitation, gel electrophoresis, and immunoblotting were done as described previously (17), with minor modifications. Purified proteins which were preincubated in the TB with 0.5% Triton X in the in vitro binding assay or cell lysates (2×10^7 cells/ml) were incubated at 4°C for 2 h with the indicated antibodies and protein A-Sepharose. The immunoprecipitates were subjected to Western blot analysis with an anti-tyrosine-phosphorylated STAT5 monoclonal Ab (anti-p-STAT5; Upstate), anti-MgcRacGAP (12), anti-importin β1 (Transduction Laboratories), or anti-MKLP-1, anti-STAT5A, anti-Rac1, or anti-importin α1 (Santa Cruz) antibodies. The filter-bound Ab were detected using the enhanced chemiluminescence system (Amersham). Cytosol and nuclear fractions were prepared, as described previously (17). Fractionation was confirmed by Western blotting with the anti-histone deacetylase (HDAC; for the nuclear fraction) or RhoA (for the cytosol fraction) Ab (Santa Cruz).

Generation of MgcRacGAP conditional knockout cells (5C cells) using DT40 cells. Full-length MgcRacGAP cDNA was cloned into the EcoRI/BamHI site of pUHD10-3 to yield a tetracycline (TET)-sensitive expression plasmid, pUHD-MgcRacGAP. For targeting constructs, a histidinol (hisD) or puromycin (puro) resistance cassette under the control of the β-actin promoter was inserted between the two arms. The targeting constructs and pUHD-MgcRacGAP were transfected into DT40 cells with a GenePulser II electroporator (Bio-Rad). DT40 cells were cultured and transfected as described previously (32). All DT40 cells were cultured at 38°C in Dulbecco's modified medium supplemented with 10% fetal calf serum, 1% chicken serum, penicillin, and streptomycin. To suppress expression of the tetracycline-responsive transgenes, TET (Sigma) was added to the culture medium at a final concentration of 2 μg/ml.

Expression constructs. Flag-tagged wild-type (WT) and mutant MgcRacGAP or STATs were cloned into EcoRI and NotI sites of a mammalian expression vector, pME 18S, or a retrovirus expression vector, pMXs-IG and pMXs-neo. The deletion constructs of MgcRacGAP that lack the internal (INT) domain or various regions of the INT domain were generated by overlapping extension using PCR as described in reference 18. Synthesized oligonucleotides encoding the NLS of MgcRacGAP (NLS-MgcRacGAP; amino acids [aa] 182 to 200), mutant NLS of MgcRacGAP (NLS-MgcRacGAP-182AAA/199AA), or the large T antigen-NLS (PKKKRKV) were cloned into EcoRI and NotI sites of a pMXs-GFP-fusion vector. Site-directed mutagenesis of MgcRacGAP or STATs was done using QuikChange (Stratagene) and the oligonucleotide primers. Several alanine substitution mutants were generated by overlapping extension using PCR. The sequence generated by PCR was confirmed by automated sequencing using an ABI Prism 310 genetic analyzer (Perkin-Elmer).

Production of retroviruses. High-titer retroviruses harboring Cre-recombinase were produced in transient retrovirus packaging cell line PLAT-E or PLAT-A (36).

Cell culture and transfection. The 293T cells were grown in Dulbecco's modified Eagle medium supplemented with 5% fetal calf serum and were transiently transfected with plasmids encoding the wild-type or the mutant forms of STATs using Lipofectamine Plus (Gibco-BRL) according to the manufacturer's recommendations.

Luciferase reporter assay. For the experiments using DT40 cells, pMKIT (mock) or pMKIT/ITD-Flt3 together with 1.0 μg of pME/STAT5A, 1.0 μg of a reporter plasmid carrying a firefly luciferase gene driven by the β-casein promoter, and 0.5 μg of an internal control reporter plasmid with the Rous sarcoma virus long terminal repeat promoter was introduced into 2×10^6 cells of 5C cells with Nucleofector II (Amaxa) set at program B-009 using the Cell Line Nucleofector kit T (Amaxa) according to the manufacturer's instruction. A control vector carrying GFP was introduced to more than 50% of 5C cells under this condition. Sixteen hours after transfection, cells were lysed and were then subjected to a dual luciferase reporter system (Promega). Luciferase activities were also examined in the lysates of 5C transfectants cotransfected with the NF-κB reporter plasmid (k9) carrying a firefly luciferase gene driven by the IL-6 promoter (14) together with an internal control plasmid. After the transfection, cells were incubated with 30 nM phorbol myristate acetate (PMA) and 1 μM ionomycin for 12 h before cell lysates were prepared. For the experiments using 293T cells, cells were transfected with pME (mock) or pME/STAT5As together with 0.5 μg of pME/EPOR, 0.5 μg of a reporter plasmid carrying a firefly luciferase gene driven by the β-casein promoter, and 0.5 μg of an internal control reporter

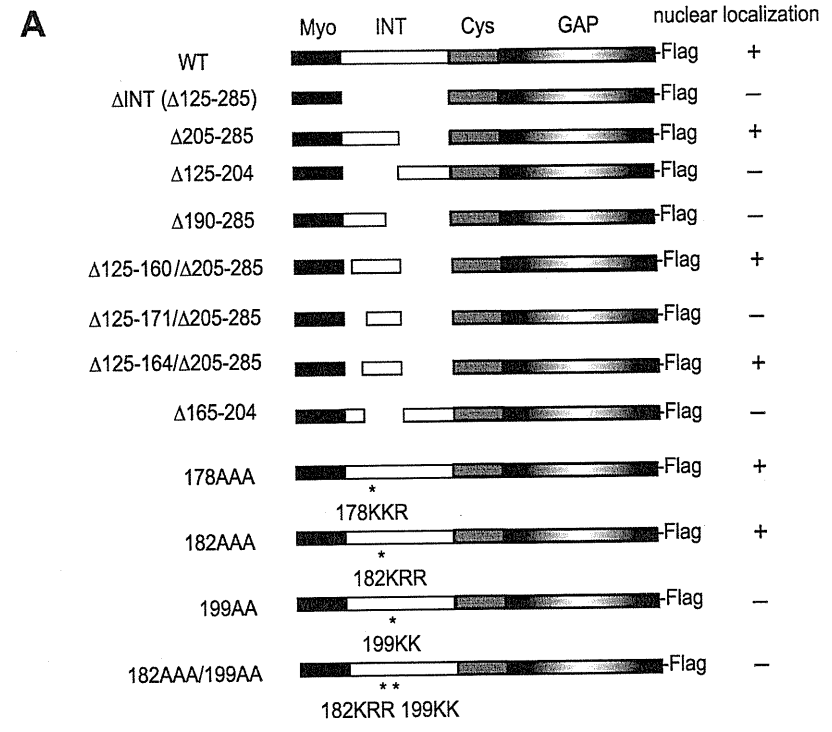
A
Myo
INT
Cys
GAP
nuclear localization
WT
Flag
+
ΔINT (Δ125-285)
Flag
–
Δ205-285
Flag
+
Δ125-204
Flag
–
Δ190-285
Flag
–
Δ125-160/Δ205-285
Flag
+
Δ125-171/Δ205-285
Flag
–
Δ125-164/Δ205-285
Flag
+
Δ165-204
Flag
–
178AAA
Flag
+
178KKR
182AAA
Flag
+
182KRR
199AA
Flag
–
199KK
182AAA/199AA
Flag
–
182KRR 199KK

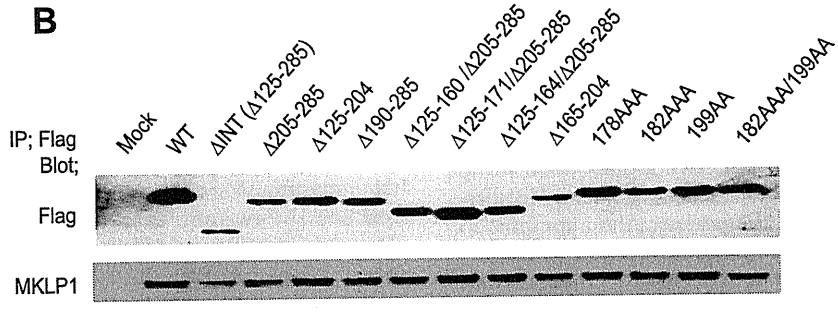
B
IP; Flag
Blot;
Flag
MKLP1
Mock
WT
ΔINT (Δ125-285)
Δ205-285
Δ125-204
Δ190-285
Δ125-160 /Δ205-285
Δ125-171/Δ205-285
Δ125-164/Δ205-285
Δ165-204
178AAA
182AAA
199AA
182AAA/199AA

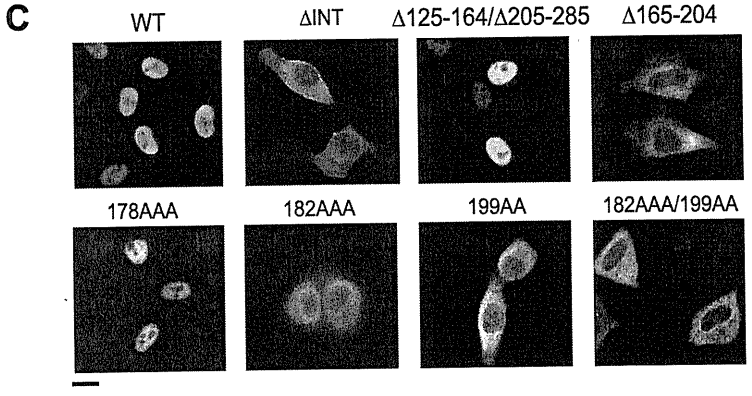
C
WT
ΔINT
Δ125-164/Δ205-285
Δ165-204
178AAA
182AAA
199AA
182AAA/199AA

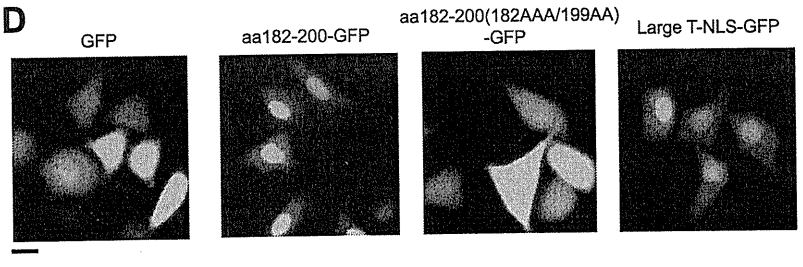
D
GFP
aa182-200-GFP
aa182-200(182AAA/199AA)
-GFP
Large T-NLS-GFP

plasmid with the Rous sarcoma virus long terminal repeat promoter, using Lipofectamine Plus (Gibco-BRL). Twenty-four hours after transfection, cells were stimulated with erythropoietin (EPO; 18 ng/ml; 16 h) and subjected to a dual luciferase reporter system (Promega). To examine the transcriptional activities of STAT3 mutants harboring deletions in DB2, a luciferase assay was done in the lysates of unstimulated or IL-6-stimulated (20 ng/ml) and sIL-6R-stimulated (20 ng/ml) 293T cells cotransfected with the STAT3 reporter plasmid carrying a firefly luciferase gene driven by the mouse glial fibrillary acidic protein promoter (35) together with an internal control reporter plasmid and either the mock vector (pME), the expression vector for the Flag-tagged WT STAT3, or a series of STAT3 mutants harboring deletions in DB2.

Semiquantitative RT-PCR. Gene expression was examined by semiquantitative reverse transcription-PCR (RT-PCR) analysis. One microgram of total RNA was reverse transcribed with random hexamers by using a first-strand cDNA synthesis kit (Pharmacia), and the reaction mixture was subjected to PCR. PCRs were carried out using the following oligonucleotide primers: chicken *Bcl-xL* sense (5′-CGTACCAGAGCTTTGAGCAGGT-3′) and antisense (5′-GACCA AGCACAAGCACAATCAC-3′) and chicken glyceraldehyde-3-phosphate dehydrogenase (*GAPDH*) sense (5′-ATGGTGAAAGTCGGAGTCAACGG-3′) and antisense (5′-ACAGTGCCCTTGAAGTGTCC-3′). PCR was performed under the following conditions to amplify the chicken *Bcl-xL* gene: 96°C for 3 min; 30 cycles of 96°C for 30 s, 63°C for 30 s, and 72°C for 30 s; a final elongation at 72°C for 8 min. To amplify the *GAPDH* gene, conditions were 96°C for 3 min, 20 cycles of 96°C for 30 s, 55°C for 30 s, and 72°C for 30 s, and a final elongation at 72°C for 8 min. Amplification of the product is not saturated at this number of cycles.

Modeling of mutant structures. The models of the D1-10, d356P, d357E, d358L, and L358A mutants of STAT3 were built using the 2.25-Å resolution crystal structure of the STAT3β · DNA complex (2) (PDB ID 1BG1) as a template. Initial models were constructed with the MODELER 9v1 program (9, 28, 41). Then, the models were refined by energy minimization with the AMBER99 force field (46) using MOE computer software (Chemical Computing Group Inc.).

RESULTS

The INT domain of MgcRacGAP contains the bipartite NLS. While endogenous MgcRacGAP localizes both in the cytoplasm and nucleus, overexpressed exogeneous MgcRacGAP mainly accumulates to the nucleus in the interphase in HeLa cells (12). Although MgcRacGAP does not harbor a classic (polybasic) NLS, we found that the ΔINT mutant localized in the cytoplasm (Fig. 1C). These results suggested that the INT domain was critical for the nuclear translocation of MgcRacGAP. To identify a functional NLS of MgcRacGAP, we produced a series of Flag-tagged deletion mutants of the INT domain (Fig. 1A). Protein expression of the mutants and their interaction with a known binding partner, MKLP-1 (34), were confirmed by immunoprecipitation and Western blotting using anti-Flag Ab and anti-MKLP-1 Ab (Fig. 1B). After the immunostaining experiments in HeLa cells, we found that aa 165 to 204 of MgcRacGAP were required for its nuclear localization (Fig. 1C). Since this region contained three polybasic regions (178KKR, 182KRR, and 199KK), we tested whether these polybasic regions could serve as an NLS. We produced alanine substitution mutants (178AAA, 182AAA, 199AA, and 182AAA/199AA) and tested their subcellular localizations. While the 178AAA mutant was located in the nucleus, the 182AAA mutant showed partial cytoplasmic localization, and the 199AA and 182AAA/199AA mutants mostly localized in cytoplasm (Fig. 1C). Next, aa182-200, aa182-200(182AAA/199AA), and a conventional NLS of large T antigen were fused to the N terminus of GFP and we viewed their subcellular localizations with a fluorescence microscope in living cells. As shown in Fig. 1D, aa182-200–GFP and large T-NLS-GFP but not GFP alone or aa182-200(182AAA/199AA)–GFP preferentially accumulated to the nucleus, indicating that aa 182 to 200 is sufficient for a functional polybasic NLS. We also confirmed that leptomycin B treatment, which inhibits nuclear export signal-dependent nuclear export by specific binding to CRM1, did not affect the nuclear or cytoplasmic localization of the WT or 182AAA/199AA mutant, respectively (data not shown). These results suggest that 182KRR and 199KK serve as a functional bipartite NLS for MgcRacGAP. Next, we asked whether MgcRacGAP was transported into the nucleus by importin family members like other proteins carrying NLS. β1Δ450-876, a mutant of importin β1 which lacks the importin α binding site, thereby competitively blocking importin α/β-mediated nuclear import (21), strongly inhibited the nuclear translocation of MgcRacGAP (data not shown). These results implied that MgcRacGAP was transported to the nucleus in an importin α/β-dependent manner.

Importin αs specifically bind MgcRacGAP in yeast through its bipartite NLS. To determine which member of the importin α family is involved in the nuclear transport of MgcRacGAP, we used a yeast two-hybrid system. To test another possibility, that importin β1 directly mediates the nuclear import of MgcRacGAP, we also examined whether importin β1 could directly bind MgcRacGAP. It was found that importin αs specifically bound MgcRacGAP in yeast (see Fig. S1A in the supplemental material). Moreover, purified importin α1 but not importin β1 pulled down MgcRacGAP from HeLa cell lysate (see Fig. S1B in the supplemental material), suggesting that importin α1 but not importin β1 directly bound MgcRacGAP. The purity of isolated importin α1 and importin β1 was confirmed by CBB staining (see Fig. S1C in the supplemental material). To determine if the bipartite NLS of MgcRacGAP indeed mediated its association with importin α1, we tested the interaction of importin α1 with the INT domain, aa 165 to 205, or each of the alanine mutants of MgcRacGAP (182AAA, 199AA, and 182AAA/199AA), and confirmed that the interaction between importin α1 and MgcRacGAP was mediated by the bipartite NLS of MgcRacGAP (see Fig. S1D in the supplemental material). These results demonstrated that MgcRac-

FIG. 1. Identification of the nuclear localization signal of MgcRacGAP. (A) Schematic diagram of various Flag-tagged deletion mutants in the INT domain of MgcRacGAP and summary of the localizations of these mutants. (B) Expression of various deletion mutants and their potential to interact with a known partner, MKLP-1. Cells were transfected with expression vectors carrying Flag-tagged WT or various deletion mutants in the INT domain. After 36 h, cells were immunoprecipitated with the anti-Flag Ab and blotted with the anti-Flag Ab (upper panel) or anti-MKLP-1 Ab (lower panel). (C) Localization of Flag-tagged WT and various deletion mutants in the INT domain of MgcRacGAP in HeLa cells. Cells were transfected with expression vectors carrying Flag-tagged WT or various deletion mutants in the INT domain. After 36 h, cells were immunostained with the anti-Flag Ab (green) and DAPI (blue) and viewed with a fluorescence microscope IX70 (Olympus). Bar, 10 μm. (D) Localization of GFP-fused NLS of MgcRacGAP. GFP-fused aa182-200 of MgcRacGAP, aa182-200(182AAA/199AA), and large T antigen-NLS were expressed in HeLa cells. After 36 h, living cells were viewed with a fluorescence IX70 microscope (Olympus). Bar, 10 μm.

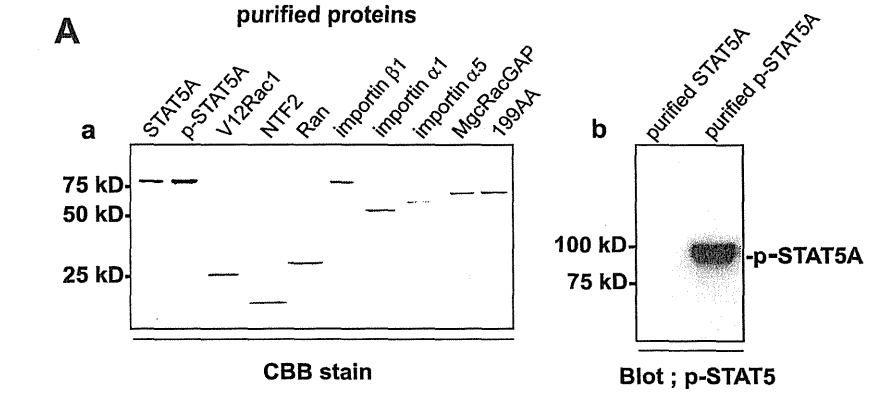
A
purified proteins
a
STAT5A
p-STAT5A
V12Rac1
NTF2
Ran
importin β1
importin α1
importin α5
MgcRacGAP
199AA
75 kD
50 kD
25 kD
CBB stain
b
purified STAT5A
purified p-STAT5A
100 kD
75 kD
-p-STAT5A
Blot ; p-STAT5

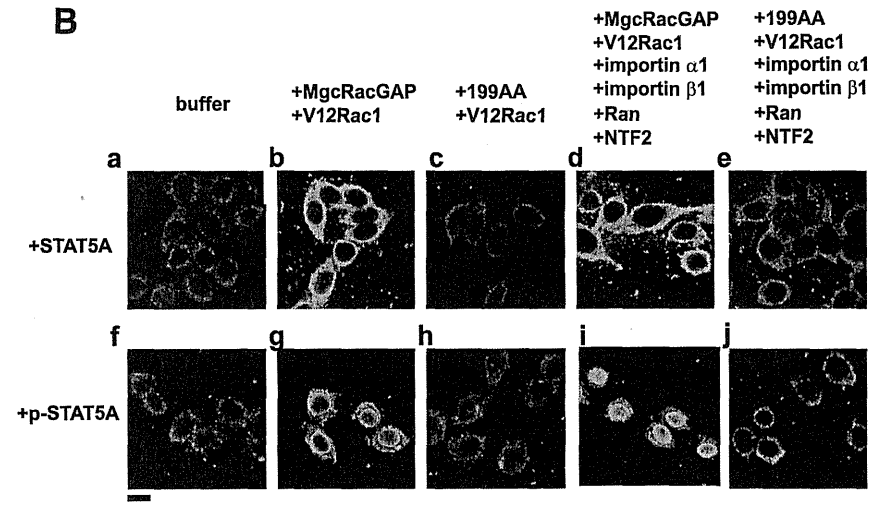
B
buffer
+MgcRacGAP
+V12Rac1
+199AA
+V12Rac1
+MgcRacGAP
+V12Rac1
+importin α1
+importin β1
+Ran
+NTF2
+199AA
+V12Rac1
+importin α1
+importin β1
+Ran
+NTF2
a
b
c
d
e
+STAT5A
f
g
h
i
j
+p-STAT5A

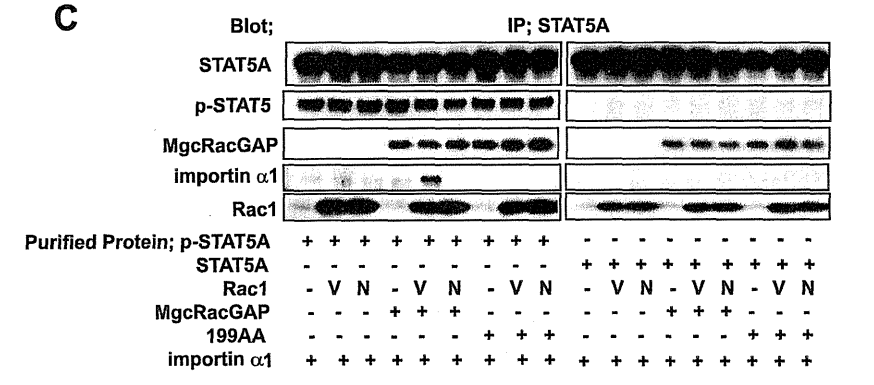
C
Blot;
IP; STAT5A
STAT5A
p-STAT5
MgcRacGAP
importin α1
Rac1
Purified Protein; p-STAT5A + + + + + + + + + - - - - - - - - -
STAT5A - - - - - - - - - + + + + + + + + +
Rac1 - V N - V N - V N - V N - V N - V N
MgcRacGAP - - - + + + - - - - - - + + + - - -
199AA - - - - - - + + + - - - - - - + + +
importin α1 + + + + + + + + + + + + + + + + + +

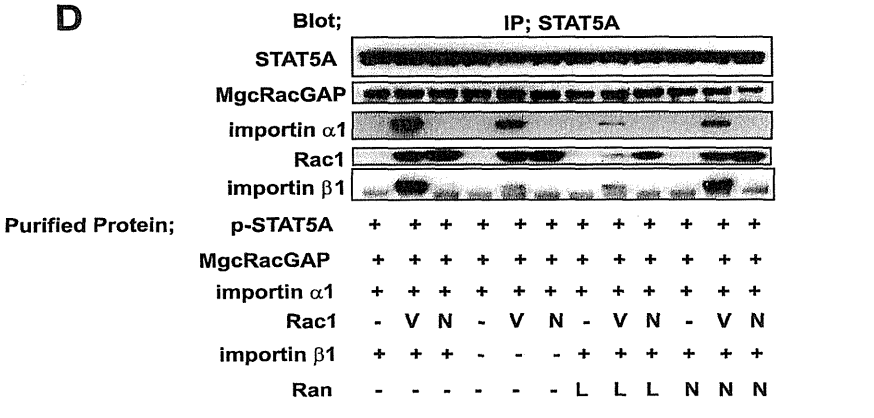
D
Blot;
IP; STAT5A
STAT5A
MgcRacGAP
importin α1
Rac1
importin β1
Purified Protein;
p-STAT5A + + + + + + + + + + + +
MgcRacGAP + + + + + + + + + + + +
importin α1 + + + + + + + + + + + +
Rac1 - V N - V N - V N - V N
importin β1 + + + - - - + + + + + +
Ran - - - - - - L L L N N N

GAP directly bound importin αs through its bipartite NLS (182KRR and 199KK).

NLSs of MgcRacGAP and GTP-bound Rac1 were required for nuclear translocation of p-STATs in the in vitro nuclear transport assay. GTP-bound Rac1 and MgcRacGAP were reported to promote nuclear translocation of p-STATs, forming a ternary complex via the importin α/β pathway in an in vitro nuclear transport assay (17), but the component of the ternary complex that directly binds importin α remained elusive. Neither STAT3 nor STAT5 harbors an apparent polybasic or PY-type NLS. One possibility is that p-STATs themselves harbor unidentified functional NLSs. However, the requirement of MgcRacGAP/GTP-Rac1 for the nuclear translocation of p-STATs raises another possibility that MgcRacGAP functions as an NLS-containing nuclear chaperone of p-STATs. We first asked if the NLS of MgcRacGAP plays a role in the nuclear translocation of p-STAT5A by using an in vitro nuclear transport assay (1). For this, Sf-9-mediated protein purification was done for WT or the 199AA mutant of MgcRacGAP, a constitutively active mutant Rac1 (V12Rac1), STAT5A, or p-STAT5A and for nuclear transporter proteins, including importin α1, importin β1, Ran, and NTF2, which binds Ran and enhances Ran-dependent nuclear import (Fig. 2A, panel a). We confirmed the purities of recombinant proteins and the tyrosine phosphorylation of STAT5A induced by coexpression with the kinase domain of JAK2 (JH1) (40) in Sf-9 cells (Fig. 2A, panels a and b). We also examined the extent of STAT5A phosphorylation by phosphate-affinity SDS-PAGE using acrylamide-pendant Phos-tag and found that about 10% was phosphorylated by coexpression of JH1 (data not shown). Although purified p-STAT5A contained only about 10% phosphorylated forms, as we previously reported (17), efficient accumulation to the nuclear envelope of p-STAT5A but not of unphosphorylated STAT5A was achieved in the presence of both purified MgcRacGAP and V12Rac1 (Fig. 2B, panels g and b), and further addition of the purified nuclear transporters, including importin α1, importin β1, Ran, and NTF2, induced efficient nuclear translocation of p-STAT5A but not of unphosphorylated STAT5A (Fig. 2B, panels i and d). Addition of the purified nuclear transporters alone was not sufficient for the nuclear translocation of p-STAT5A, and the addition of purified dominant negative N17Rac1 instead of V12Rac1 blocked the nuclear translocation of p-STAT5A even in the presence of purified MgcRacGAP and other nuclear transporters (data not shown). Notably, 199AA-MgcRacGAP did not support the accumulation of p-STAT5A at the nuclear envelope, even in the presence of V12Rac1, and abolished the nuclear translocation of p-STAT5A even in the presence of V12Rac1, importin α1, importin β1, Ran, and NTF2 (Fig. 2B, panels h and j).

To determine if both the NLS of MgcRacGAP and Rac1 activation are required for complex formation of p-STAT5A with importin α, an in vitro binding assay was done. As we reported previously (17), p-STAT5A, but not unphosphorylated STAT5A, formed complexes with importin α1 only in the presence of WT MgcRacGAP and V12Rac1 (Fig. 2C). On the other hand, p-STAT5A did not form complexes with importin α1 in the presence of 199AA-MgcRacGAP and V12Rac1 (Fig. 2C). Addition of importin β1 increased the amount of importin α1 associating with the complex of p-STAT5A, WT MgcRacGAP, and V12Rac1, and further addition of GTP-bound Ran (L69Ran) but not GDP-bound Ran (N24Ran) dissociated the import complex (Fig. 2D), suggesting that Ran was indeed involved in the nuclear import of p-STAT5A. We also found that 199AA-MgcRacGAP did not support the nuclear translocation of p-STAT3 in the presence of V12Rac1, importin α1, importin β1, Ran, or NTF2 (see Fig. S2 in the supplemental material). Conversely, addition of purified p-STATs and V12Rac1 was required for the nuclear import of GST-MgcRacGAP in the presence of purified importin α/β pathway proteins (see Fig. S3A and B in the supplemental material). These results suggested that the NLS of MgcRacGAP was somehow activated by the association with p-STATs and GTP-bound Rac1, and bound importin α, thereby facilitating nuclear transport of the MgcRacGAP/p-STATs/Rac1 complex. Altogether, the present results indicate that the bipartite NLS was essential for MgcRacGAP to function as a nuclear chaperone of p-STATs, in accordance with GTP-bound Rac1, at least in the in vitro nuclear transport assay.

Generation of MgcRacGAP conditional knockout DT40 cells, in which expression of exogenous MgcRacGAP is under control of a tetracycline-repressible promoter. To determine if the 199AA or 182AAA/199AA mutant could alter the tran-

FIG. 2. Nuclear translocation of p-STAT5A requires the NLS of MgcRacGAP. (A) The recombinant proteins used in the experiments are shown, after CBB staining of purified proteins (a) or Western blot analysis of the STAT5A-Flag protein purified from Sf-9 cells with or without coexpression with the kinase domain of JAK, using the anti-p-STAT5 Ab (b). (B) Nuclear transport assay of STAT5A. HeLa cells were permeabilized using 40 μg/ml digitonin and were incubated at 37°C for 30 min with 50 μl IM. The IM contained TB, ERS, and a single protein or combinations of the following purified proteins, as indicated: 1 μM STAT5A, p-STAT5A, V12Rac1, MgcRacGAP, 199AA-MgcRacGAP, importin α1, importin β1, Ran, or NTF2. After the import reaction, the cells were fixed. STAT5A protein was detected using the anti-STAT5A Ab. Cells were examined using a FLUOVIEW FV300 confocal microscope (Olympus). A representative result of three independent experiments is shown. Bar, 10 μm. (C) The ternary protein complex composed of p-STAT5A, GTP-bound Rac1, and 199AA-MgcRacGAP did not bind importin α1 in the transport buffer. Purified STAT5A and p-STAT5A were incubated with importin α1 in the absence or presence of the indicated combinations of V12Rac1, N17Rac1, MgcRacGAP, or 199AA-MgcRacGAP in the transport buffer containing 5% bovine serum albumin for blocking nonspecific binding. One microgram of each purified protein was used for each sample. After the incubation, STAT5A was immunoprecipitated (IP) with anti-STAT5A Ab and washed three times with transport buffer. The immunoprecipitates were subjected to Western blot analysis with the anti-importin α1, anti-Rac1, anti-MgcRacGAP, anti-STAT5A Ab, or anti-p-STAT5A Ab. (D) GTP-bound Ran (L69Ran) dissociates Rac1, importin α1, and importin β1 from the import complex composed of p-STAT5A. Purified p-STAT5A was incubated with purified V12Rac1, MgcRacGAP, and importin α1 in the presence of the indicated combinations of purified importin β1 alone, importin β1 plus Q69Ran (GTP-bound Ran), or importin β1 plus N24Ran (GDP-bound Ran) in the transport buffer containing 5% bovine serum albumin for blocking nonspecific binding. One microgram of each purified protein was used for each sample. After the incubation, STAT5A was immunoprecipitated with anti-STAT5A Ab and washed three times with transport buffer. The immunoprecipitates were subjected to Western blot analysis with the anti-importin α1, anti-Rac1, anti-MgcRacGAP, anti-importin β1, or anti-STAT5A Ab.

A
Tet ; 0 3h 6h 9h 12h
MgcRacGAP
Tubulin
Cell; 5C cells (MgcRacGAP-/-/MgcRacGAP transgene)
B
Tet (+) 12h
5C/mock
5C/WT
Red; actin
Blue; DAPI
C
Tet - Tet +
C N C N C N C N
G-CSF; - - + + - - + +
p-STAT3
MgcRacGAP
RhoA
HDAC
Tet - Tet +
G-CSF; - + - +
Total western
D
cell number (10^4)
1000
100
10
1
1 2 3
days
MOCK
WT
199AA
182AAA
182AAA/199AA
E
blot; mock WT 182AAA 199AA 182AAA/199AA
Flag
loading control; α-tubulin
F
WT 182AAA 199AA 182AAA/199AA
G-CSF; - + - + - + - +
p-STAT3
STAT3
G
WT 182AAA 199AA 182AAA/199AA
C N C N C N C N C N C N C N C N
G-CSF; - - + + - - + + - - + + - - + +
p-STAT3
Flag (MgcRacGAP)
RhoA
HDAC
H
WT 182AAA 199AA 182AAA/199AA
G-CSF; - + - + - + - +
Bcl-XL
GAPDH

scriptional activation of STATs in vivo, we first performed a luciferase assay using 293T cells. The IL-6-induced activation of STAT3 was clearly enhanced by cotransfection with the wild-type MgcRacGAP (~45-fold, compared with mock transfection [~10-fold]). Unexpectedly, cotransfection of the 199AA or 182AAA/199AA mutant modestly inhibited the IL-6-induced transactivation of STAT3 (~25-fold) compared with WT but, rather, enhanced it when compared with mock treatment (data not shown). It is possible that these MgcRacGAP mutants form a heterodimer with endogenous MgcRacGAP and that the heterodimer but not the homodimer of the 199AA or 182AAA/199AA mutant enhanced IL-6-induced transcriptional activation of STAT3. To exclude the effects of endogenous MgcRacGAP, we attempted to establish an MgcRacGAP conditional knockout using DT40 cells. We generated DT40 mutants in which cells with a disrupted MgcRacGAP gene were sustained by expression of the exogenous MgcRacGAP cDNA under the control of a tetracycline-repressible promoter. As shown in Fig. S4A in the supplemental material, an MgcRacGAP-targeting construct was generated such that the 8.0-kb genomic fragment encoding the open reading frame was replaced with one of the two selection cassettes. We transfected the MgcRacGAP-targeting construct containing the histidinol resistance cassette into DT40 cells and isolated MgcRacGAP$^{+/-}$ clones. One MgcRacGAP$^{+/-}$ clone was cotransfected with a chicken MgcRacGAP transgene under the control of a TET-repressible promoter and a TET-repressible transactivator containing a zeocin (ZEO) resistance cassette. We selected ZEO-resistant colonies and identified several clones carrying these constructs integrated at random sites in the genome (MgcRacGAP$^{+/-/\text{MgcRacGAP transgene}}$). Five clones with the MgcRacGAP$^{+/-/\text{MgcRacGAP transgene}}$ genotype were transfected with another MgcRacGAP-targeting construct harboring a puromycin selection marker to disrupt the remaining MgcRacGAP allele. We obtained 24 clones with the MgcRacGAP$^{-/-/\text{MgcRacGAP transgene}}$ genotype, and one clone, 5C, was chosen for further analysis (see Fig. S4B, panels a and b, in the supplemental material). Exogenous MgcRacGAP protein under the control of a TET-repressible promoter in 5C cells was not detected by Western blot analysis with anti-chicken MgcRacGAP Ab at 6 to 12 h after addition of TET, indicating that a TET-repressible promoter of this clone worked successfully and that MgcRacGAP was actively turned over (Fig. 3A). When the expression of the MgcRacGAP transgene was suppressed by adding TET, cell growth of 5C cells was suppressed together with the inhibition of cytokinesis, and the cells formed multinucleated cells, eventually undergoing apoptosis within 48 h (Fig. 3B and data not shown). This phenotype is consistent with the previous result indicating that MgcRacGAP is required for completion of cytokinesis.

The 199AA and 182AAA/199AA mutants inhibited nuclear translocation and transcriptional activation of p-STAT3 in MgcRacGAP knockout cells. To determine if MgcRacGAP is required for the nuclear translocation of p-STAT3 in vivo, we investigated whether depletion of MgcRacGAP affected the subcellular distribution of p-STAT3 after granulocyte colony-stimulating factor (G-CSF) stimulation using the 5C cells. The 5C cells, which had been transiently transfected with a vector carrying a G-CSF receptor, were treated with TET for 4 h and were stimulated with G-CSF (15 min), followed by nuclear-cytosol fractionation analysis. We also confirmed that after treatment with TET for 4 h only a portion of the 5C cells formed multinucleated cells (less than 10%) (data not shown). The nuclear-cytosol fractionation analysis revealed that depletion of MgcRacGAP resulted in a decreased amount of the G-CSF-induced p-STAT3 as well as inhibition of the nuclear accumulation of p-STAT3 (Fig. 3C). These results implied that MgcRacGAP mediates the G-CSF-induced phosphorylation

FIG. 3. The NLS of MgcRacGAP is required for the transcriptional activation of p-STAT3 in 5C cells. (A) Suppression of MgcRacGAP by TET in 5C cells. The 5C cells were treated with TET for the time indicated and lysed. Cell lysates were separated on SDS-PAGE and immunoblotted with the anti-chicken MgcRacGAP Ab (upper panel) or anti-α-tubulin Ab (lower panel). (B) Flag-tagged WT MgcRacGAP rescued 5C cells from becoming multinucleated after addition of TET. The 5C cells transduced with mock or Flag-tagged WT were stained with rhodamine-conjugated phalloidin (red) and DAPI (blue) 12 h after the addition of TET and viewed using a FLUOVIEW FV300 confocal microscope (Olympus). Bar, 10 μm. (C) Subcellular localization of p-STAT3 in 5C cells after addition of TET in the absence or presence of G-CSF. Cell fractionation was performed using 5C cells transiently transfected with the expression vector for the G-CSF receptor (G-CSFR). Twenty-four hours after transfection, live cells were isolated using Ficoll-Paque Plus (Amersham) and used for further analysis. Cells were treated or untreated with TET for 4 h and were incubated with 100 ng/ml of G-CSF for 15 min before cell fractionations. Fractionated samples were then subjected to Western blotting with anti-p-STAT3, anti-Flag, anti-RhoA, or anti-HDAC Ab (upper panels). The total amount of p-STAT3 was also examined using whole-cell lysates of 5C cells by Western blotting with anti-p-STAT3 (lower panel). C, cytosol; N, nuclear. (D) Effect of NLS mutants of MgcRacGAP on cell proliferation. Flag-tagged WT or various MgcRacGAP mutants (182AAA, 199AA, and 182AAA/199AA) were transduced into 5C cells by using a retrovirus vector, pMXs-IG. GFP-positive cells were selected by addition of TET. The number of transfectants was counted at the indicated time points after selection. GFP-positive mock-transduced cells, which were analyzed using fluorescence-activated cell sorting, were used as a control. (E) Expression levels of the Flag-tagged WT or mutant MgcRacGAPs in 5C transfectants. Cell lysates from 5C cells expressing mock, WT, or mutant MgcRacGAPs (1×10^7/lane) were examined by Western blotting using the anti-Flag M2 monoclonal antibody (upper panel) or anti-α-tubulin Ab (lower panel). (F) G-CSF-induced phosphorylation of STAT3 in 5C cells expressing Flag-tagged WT or mutant MgcRacGAPs. The 5C cells expressing WT or mutant MgcRacGAPs cotransfected with the expression vector for G-CSFR were stimulated with 100 ng/ml of G-CSF for 15 min in the presence of TET, followed by Western blotting (5×10^6 cells/lane) using the anti-p-STAT3 antibody (upper panel) or anti-STAT3 Ab (lower panel). (G) Subcellular localization of p-STAT3 in 5C cells expressing Flag-tagged WT, 182AAA, 199AA, or 182AAA/199AA with or without G-CSF stimulation in the presence of TET. Cell fractionation was performed using 5C transfectants cotransfected with the expression vector for G-CSFR. Twenty-four hours after transfection, live cells were isolated using Ficoll-Paque Plus (Amersham) and used for further analysis. Cells were incubated with 100 ng/ml of G-CSF for 15 min before cell fractionations. Fractionated samples were then subjected to Western blotting with anti-p-STAT3, anti-Flag, anti-RhoA, or anti-HDAC Ab. (H) G-CSF-induced transcriptional activation of STAT3 was suppressed by depletion of MgcRacGAP. Expression of Bcl-xL or GAPDH mRNA was examined in the 5C transfectants expressing WT, 182AAA, 199AA, or 182AAA/199AA with or without G-CSF stimulation. Cells transiently transfected with G-CSFR were serum starved with or without G-CSF stimulation for 7 h in the presence of TET, followed by semiquantitative RT-PCR.

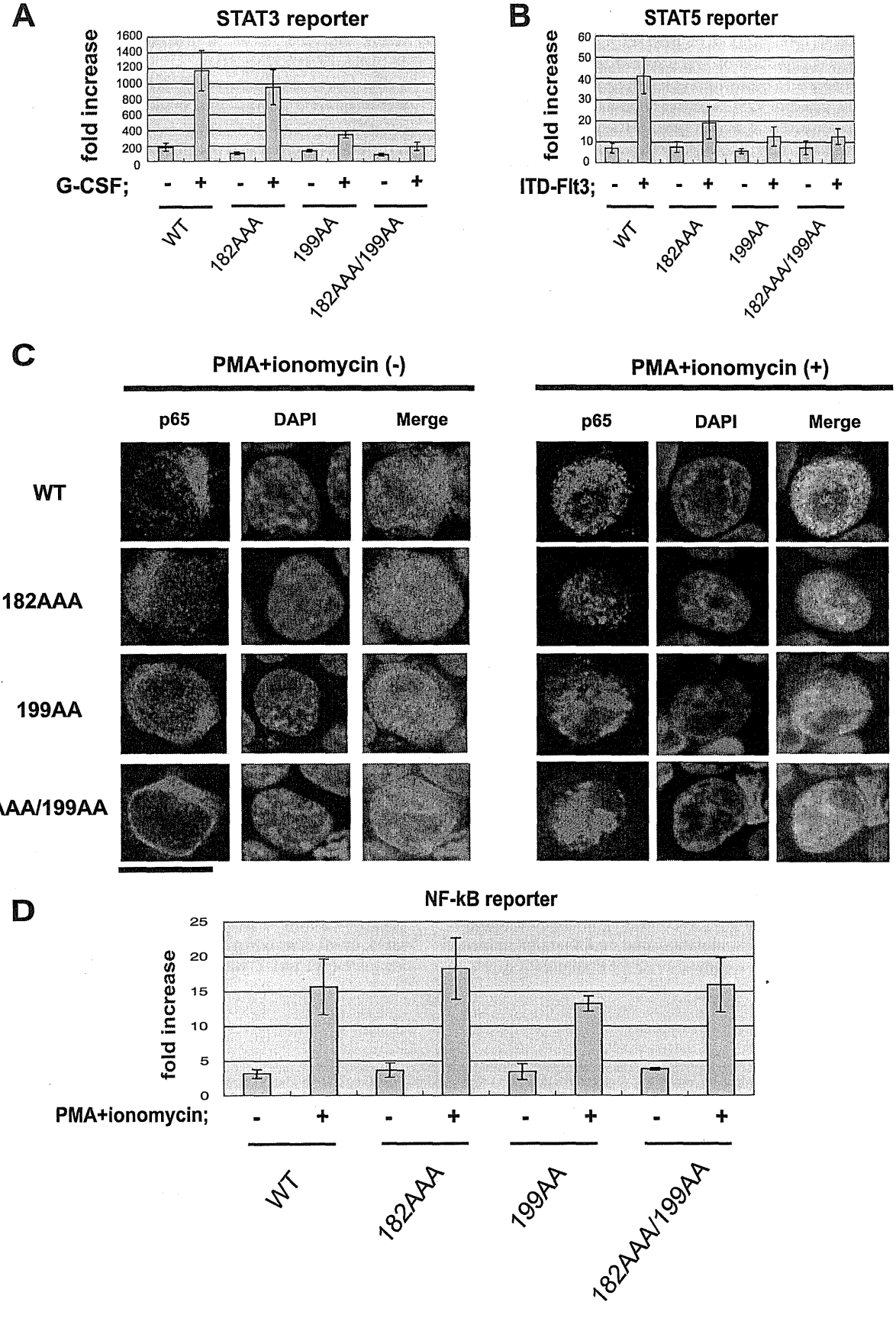
A
STAT3 reporter
fold increase
1600
1400
1200
1000
800
600
400
200
0
G-CSF; - + - + - + - +
WT
182AAA
199AA
182AAA/199AA
B
STAT5 reporter
fold increase
60
50
40
30
20
10
0
ITD-Flt3; - + - + - + - +
WT
182AAA
199AA
182AAA/199AA
C
PMA+ionomycin (-)
PMA+ionomycin (+)
p65
DAPI
Merge
WT
182AAA
199AA
182AAA/199AA
D
NF-kB reporter
fold increase
25
20
15
10
5
0
PMA+ionomycin; - + - + - + - +
WT
182AAA
199AA
182AAA/199AA

and nuclear translocation of p-STAT3. Alternatively, it was possible that depletion of MgcRacGAP indirectly affected activation of STAT3 by disturbing cell cycle machineries. Next, to avoid this possibility, 5C cells were infected with mock or the retrovirus expression vector pMXs-IG carrying WT or the 182AAA, 199AA, or 182AAA/199AA mutant of MgcRacGAP using amphotropic packaging PLAT-A cells (36). The infection efficiencies of these cells were around 10 to 30%, as assessed from the coexpression of GFP using an internal ribosome entry site sequence. After addition of TET, GFP-positive cells grew from the 5C cells transduced with WT or the mutants, while all of the mock-transduced cells became multinucleated, indicating cytokinesis failure, and eventually underwent apoptosis (Fig. 3B and data not shown). These results indicated that the cytokinesis failure of 5C cells after adding TET was prevented by either expression of the WT MgcRacGAP or NLS mutants of MgcRacGAP. All of the 182AAA-, 199AA-, or 182AAA/199AA-expressing cells grew slower than the WT-expressing cells in the presence of TET (Fig. 3D), suggesting that the NLS of MgcRacGAP plays some role in enhancing cell growth but is dispensable for completion of cytokinesis in 5C cells. Expression levels of WT MgcRacGAP or 182AAA, 199AA, or 182AAA/199AA mutant were comparable as assessed in Western blot analyses (Fig. 3E). We next investigated whether disruption of the NLS of MgcRacGAP affected the subcellular distribution of endogenous p-STAT3 after G-CSF stimulation by using the 5C transfectants in the presence of TET. The 5C cells expressing WT MgcRacGAP or the 199AA or 182AAA/199AA mutant, which had been transiently transfected with a vector carrying the G-CSF receptor, were stimulated with G-CSF (15 min). The amounts of G-CSF-induced p-STAT3 in 5C transfectants expressing the WT and those expressing the NLS-lacking mutants were found to be comparable (Fig. 3F). Interestingly, the nuclear-cytosol fractionation analysis revealed that the 199AA- or 182AAA/199AA-MgcRacGAP hardly entered the nucleus, and the G-CSF-induced nuclear accumulation of p-STAT3 was strongly inhibited in 199AA- or 182AAA/199AA-expressing cells compared with those in the 182AAA- and WT-expressing cells (Fig. 3G). We also performed a semiquantitative RT-PCR analysis to test if induction of Bcl-xL mRNA (one of the target genes of STAT3) was affected in the transfectants expressing the NLS-lacking mutants of MgcRacGAP after the G-CSF stimulation, and we found that induction of Bcl-xL mRNA in response to G-CSF stimulation was severely impaired in the transfectants expressing 199AA or 182AAA/199AA (Fig. 3H).

The 199AA and 182AAA/199AA mutants specifically blocked transcriptional activation of p-STATs in MgcRacGAP knockout cells. Next, we performed a luciferase assay using the 5C transfectants cultured in the presence of TET. Transcriptional activities of STAT3 in response to G-CSF stimulation were strongly inhibited in the 199AA- or 182AAA/199AA-expressing 5C cells compared to those in the WT-expressing cells (Fig. 4A). We obtained similar results for STAT5; transcriptional activation of STAT5 induced by ITD-Flt3 was profoundly inhibited in the 199AA- or 182AAA/199AA-expressing 5C cells compared to those in the WT-expressing cells (Fig. 4B). However, NF-κB p65, whose NLS is unmasked by IκBα degradation and binds importins α3 and α4 (8, 23), entered the nucleus after stimulation even in the 199AA- or 182AAA/199AA-expressing cells (Fig. 4C). In addition, transcriptional activities of NF-κB in response to stimulation with PMA/ionomycin were not affected in the 199AA- or 182AAA/199AA-expressing 5C cells compared to those in the WT-expressing cells (Fig. 4D), indicating that MgcRacGAP does not work as a general nuclear chaperone.

The series of STAT3 mutants harboring deletions in the two strands (βa′ and βb) of the β-barrel lost transcriptional activities, while the mutants harboring deletions in the region following the strand βb (βb-βc loop) showed constitutively active phenotypes. We previously found that STAT3 and STAT5 directly bound MgcRacGAP through aa 338 to 362 and aa 341 to 365 in their DNA binding domain, respectively (termed DB2-STAT3 and DB2-STAT5) and that the STAT3 and STAT5A mutants lacking DB2 (STAT3-dDB2 and STAT5A-dDB2) lost not only the capability for binding to MgcRacGAP but also their transcriptional activities (17). The DB2 region is well-conserved among STAT family proteins. In this study, we produced a series of deletion mutants lacking a three-amino-acid stretch in the DB2-STAT3 region (STAT3-dD1 to -8) and in the next six amino acids (STAT3-dD9 and -10) (Fig. 5A). Tyrosine phosphorylation of STAT3-dDB2, -dD1, -dD3, -dD4, or -dD5 in response to IL-6 stimulation was diminished, whereas tyrosine phosphorylation of STAT3-dD2 was prominent even in the absence of IL-6 (Fig. 5C, middle panel). In addition, association of STAT3-dDB2, -dD1, -dD3, -dD4, or -dD5 with MgcRacGAP was not detected, while binding of STAT3-dD2 with MgcRacGAP increased compared

FIG. 4. The NLS of MgcRacGAP is not required for activation of NF-κB p65 in 5C cells. (A) The NLS of MgcRacGAP was required for transcriptional activities of STAT3. Luciferase activities were examined in the lysates of 5C transfectants cotransfected with the STAT3 reporter plasmid, internal control plasmid, expression vector for the G-CSF receptor, or expression vector for the WT-STAT3 (pME/STAT3). After the transfection, cells were incubated with 100 ng/ml of G-CSF for the last 12 h before cell lysates were prepared. Cell lysates were then subjected to a dual luciferase reporter system (Promega). The results shown are the averages ± standard deviations of three independent experiments. (B) The NLS of MgcRacGAP was required for transcriptional activities of STAT5. This experiment was identical to that in panel A, except that 5C transfectants were cotransfected with the STAT5 reporter plasmid, internal control plasmid, or expression vector for the WT STAT5A (pME/STAT5A), together with either the mock or expression vector for ITD-Flt3. (C) The NLS of MgcRacGAP is dispensable for the nuclear translocation of NF-κB p65 in 5C cells. Immunostaining was performed using the 5C transfectants cotransfected with the expression vector for NF-κB p65. After the transfection, cells were serum starved for 3 h, incubated with 30 nM PMA and 1 μM ionomycin for 30 min, and stained with the anti-NF-κB p65 and DAPI. Cells were viewed with a FLUOVIEW FV300 confocal microscope (Olympus). Bar, 10 μm. (D) The NLS of MgcRacGAP was dispensable for transcriptional activities of NF-κB. Luciferase activities were examined in the lysates of 5C transfectants cotransfected with the NF-κB reporter plasmid (k9) carrying a firefly luciferase gene driven by the IL-6 promoter together with the internal control plasmid. After the transfection, cells were incubated with 30 nM PMA and 1 μM ionomycin for 12 h before cell lysates were prepared. Cell lysates were then subjected to a dual luciferase reporter system (Promega). The results shown are the averages ± standard deviations of three independent experiments.

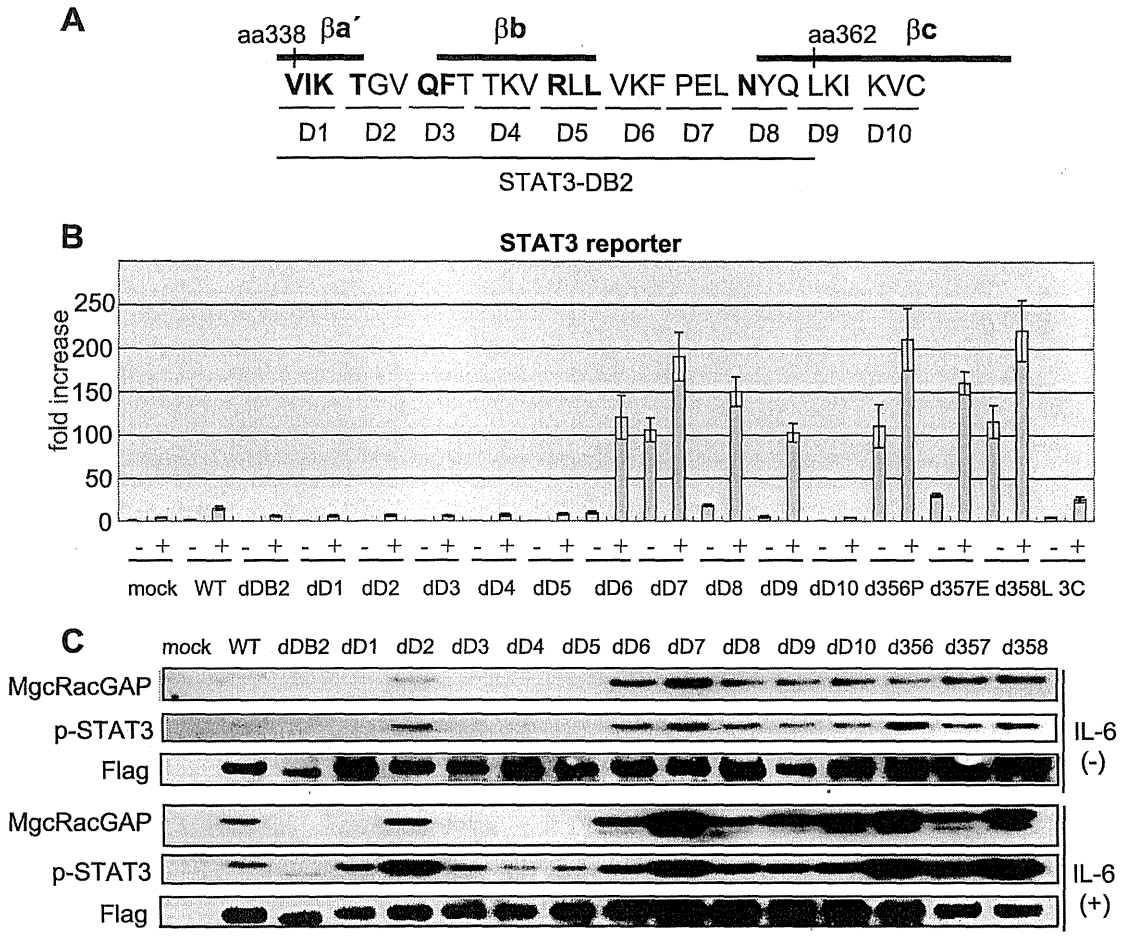

FIG. 5. Correlation between binding abilities of STAT3 to MgcRacGAP and activities of STAT3. (A) Schematic diagrams showing a series of the deletion sites of STAT3 mutants. (B) Transcriptional activities of STAT3 mutants harboring deletions in DB2. Luciferase activity was examined as described in Materials and Methods. As a control, a reported constitutively active mutant of STAT3C was used. The results shown are the averages ± standard deviations of three independent experiments. (C) MgcRacGAP binding abilities of the STAT3 mutants. Tyrosine phosphorylation and binding affinity to MgcRacGAP of Flag-tagged deletion mutants of DB2-STAT3 in the absence or presence of IL-6-stimulation were determined by immunoprecipitation using the anti-Flag Ab followed by Western blotting with the anti-p-STAT3, anti-MgcRacGAP, or anti-Flag Ab. Expression, tyrosine phosphorylation, and interaction with MgcRacGAP of the Flag-tagged deletion mutants of DB2-STAT3 (lower panel, middle panel, and upper panel, respectively) were examined by immunoprecipitation using 293T cells transfected with each of the STAT3 mutants in the absence (upper three panels) or presence (lower three panels) of IL-6-stimulation for 30 min.

with that of WT in the absence or presence of IL-6 stimulation (Fig. 5C, upper panels). Nonetheless, the mutants lacking D1 to -5 (STAT3-dD1 to -5), including STAT3-dD2, did not show detectable transcriptional activities in response to IL-6 stimulation (Fig. 5B). Surprisingly, STAT3-dD6 to -9 mutants exerted considerable transcriptional activities even without cytokine stimulation, and this was further enhanced by IL-6 stimulation (Fig. 5B). These mutants were constitutively tyrosine phosphorylated, and their tyrosine phosphorylation was augmented after IL-6 stimulation (Fig. 5C). STAT3-dD10 was constitutively tyrosine phosphorylated but did not show detectable transcriptional activities, as was the case for STAT3-dD2. We next examined whether these STAT3 mutants harbored the DNA binding activities in an electrophoretic mobility shift assay using unstimulated 293T cells and found that unlike the other constitutively tyrosine-phosphorylated STAT3 mutants, STAT3-dD2 and STAT3-dD10 lost their DNA binding affinities (data not shown). Notably, STAT3-dD7 showed the strongest transcriptional activities in the absence of cytokine stimulation among the STAT3-dD1 to -10 mutants, and its transcriptional activities in the absence of cytokine stimulation were much stronger than that of the WT after IL-6 stimulation (Fig. 5B). We next produced a series of mutants lacking each single amino acid of the three amino acids in the region of D7 (STAT3-d356P, -d357E, and -d358L). Interestingly, STAT3-d356P, -d357E, and -d358L, which strongly bound MgcRacGAP, displayed the constitutive activities in the absence of IL-6 stimulation (Fig. 5B and C). STAT3-d356P and STAT3-d358L exerted the strongest transcriptional activity among these mutants and a reported constitutively active mutant of STAT3C (3). These results suggest that the two strands (βa′ and βb) in DB2 are required for the IL-6-induced tyrosine phosphorylation of STAT3 that mediates the interaction with MgcRacGAP, whereas the deletion mutants in the C terminus

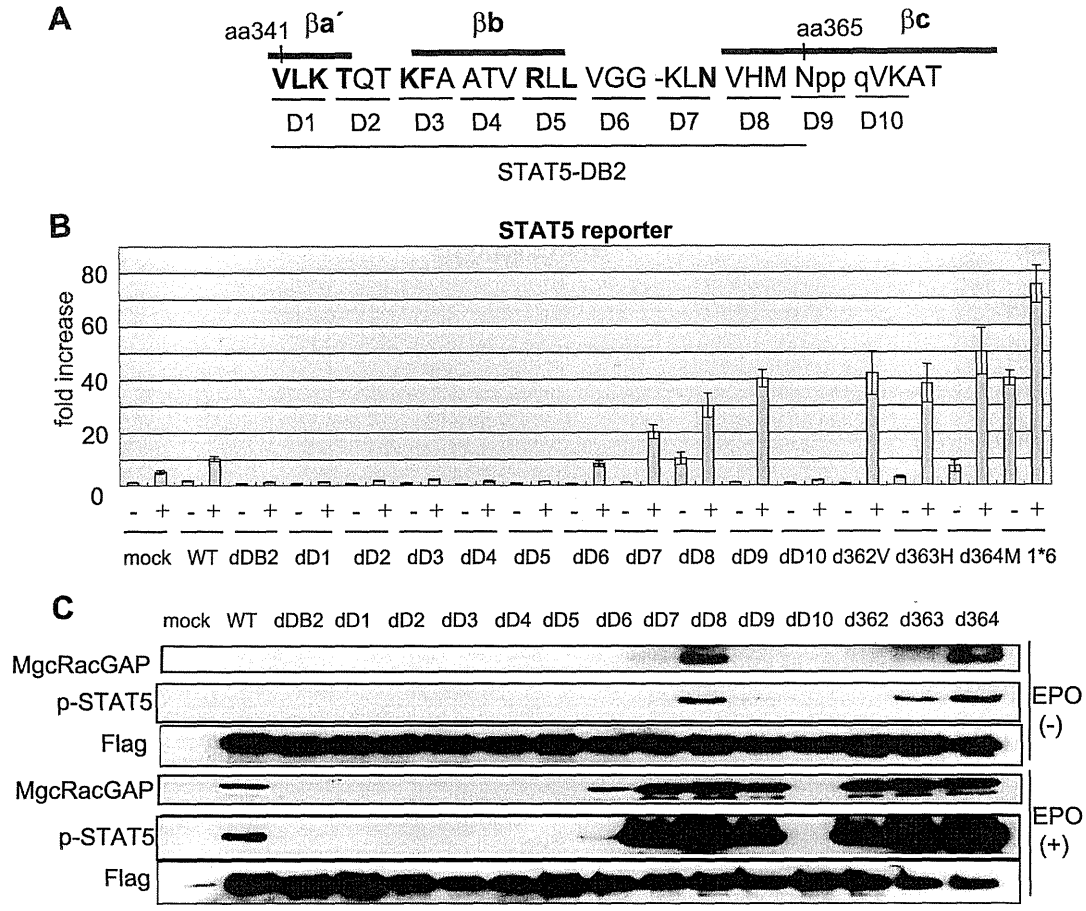

FIG. 6. The series of deletion mutants of STAT5A in DB2 showed similar phenotypes to those of STAT3. (A) Schematic diagrams showing a series of the deletion mutants of STAT5A. (B) The mutants lacking D1 to -5 and D10 (STAT5A-dD1 to -5 and STAT5A-dD10) as well as the STAT5A-dDB2 lacked their transcriptional activities even under EPO stimulation. Luciferase activity was examined in the lysates of unstimulated or EPO (18 ng/ml)-stimulated 293T cells cotransfected with the expression vector for the EPO receptor (EPOR) and STAT5 reporter plasmid together with internal control reporter plasmids and either the mock vector (pME), the expression vector for the Flag-tagged WT STAT5A, or a series of STAT5A mutants harboring deletions in DB2. As a control, the constitutively active STAT5A1*6 mutant was used. The results shown are the averages ± standard deviations of three independent experiments. (C) The mutants of STAT5A harboring deletions in the two strands (βaprime] and βb) lost binding affinities to MgcRacGAP or did not undergo tyrosine phosphorylation, while the mutants harboring deletions in the region following the strand βb showed enhanced binding affinities to MgcRacGAP and underwent enhanced tyrosine phosphorylation. Expression, tyrosine phosphorylation, and interaction with MgcRacGAP of the Flag-tagged deletion mutants of DB2-STAT5A (lower panel, middle panel, and upper panel, respectively) were examined by immunoprecipitation using 293T cells cotransfected with EPOR and each of the STAT5A mutants in the absence (upper three panels) or presence (lower three panels) of EPO stimulation for 30 min.

of DB2 following the strand βb (βb-βc loop) tend to become constitutively active with enhanced binding to MgcRacGAP.

We also produced a series of STAT5A mutants lacking a three-amino-acid stretch in the region corresponding to DB2-STAT3 (STAT5A-dD1 to -8) and in the next six amino acids (STAT5A-dD9 and -10) (Fig. 6A). We found that the series of deletion mutants of STAT5A in DB2 showed phenotypes similar to those of STAT3 mutants (Fig. 6B and C); STAT5A mutants harboring deletions in the two strands (βa′ and βb) of the β-barrel (STAT5A-dD1 to -5) were not tyrosine phosphorylated by EPO stimulation and lost transcriptional activity, while the mutants harboring deletions in the region following the strand βb (STAT5A-dD7 to -9) showed gain-of-function phenotypes. STAT5A-dD8, -d363H, and -d364M also showed constitutively active phenotypes (Fig. 6B and C), although the transcriptional activities of these mutants without stimulation were weaker than that of another constitutively active mutant, STAT5A1*6 (37). Constitutive activities of STAT5A mutants were well-correlated with constitutive binding to MgcRacGAP. Association between the constitutively active STAT5A mutants and MgcRacGAP was stronger than that of the WT and MgcRacGAP in the absence of EPO stimulation (Fig. 6C). Thus, the molecular basis of the STAT-MgcRacGAP interaction is well-conserved between STAT3 and STAT5A.

The constitutively active mutant STAT3-d358L promoted cell proliferation of a mutant cell line derived from BaF-BO3 cells. We next examined whether STAT3-d358L was biologically functional, showing physiological roles of STAT3 activation. It has been reported that BaF-BO3 cells expressing a G-CSF receptor mutant (G133 cells) are able to proliferate in

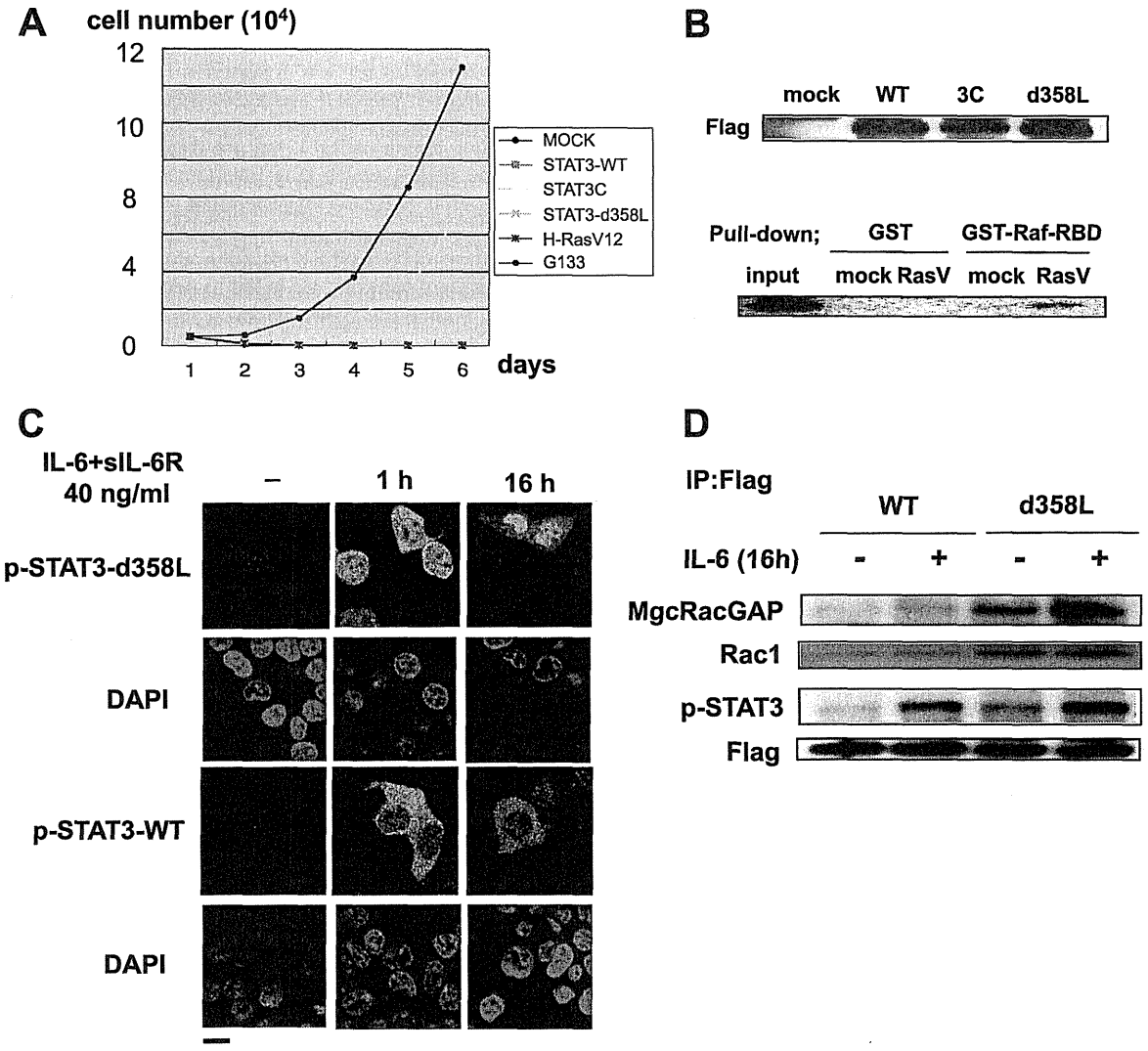

FIG. 7. A constitutively active STAT3 mutant, STAT3-d358L, preferentially bound MgcRacGAP and Rac1 and accumulated to the nucleus. (A) STAT3-d358L supports proliferation of BaF-BO3-G133F3 cells in the presence of G-CSF. BaF-BO3-G133F3 cells expressing mock vector or the Flag-tagged WT STAT3, STAT3C, STAT3-d358L, or H-RasV12 were cultured in the presence of G-CSF, and the cell numbers were determined at the indicated times. BaF-BO3-G133 cells were used as a control. (B) Similar expression levels of WT STAT3, STAT3C, and STAT3-d358L were confirmed by Western blotting with the anti-Flag Ab (upper panel). The expression and activation of H-RasV12 were examined by Western blotting with the anti-Flag Ab (lower panel; input lane) and by pull-down assay using GST–Raf-RBD (lower panel; other lanes), respectively. (C) The STAT3-d358L mutant preferentially accumulated to the nucleus. 293T cells were transfected with pME/STAT3-d358L-Flag (upper panels) or pME/WT-STAT3-Flag (lower panels). After 24 h, the cells were stimulated with IL-6 for the time indicated and fixed, followed by immunostaining with the anti-p-STAT3 or anti-Flag Ab (data not shown). Bar, 10 μm. (D) STAT3-d358L constitutively bound MgcRacGAP and Rac1. Interaction of MgcRacGAP or Rac1 with WT STAT3 or STAT3-d358L was examined by coimmunoprecipitation (IP) using 293T cells transfected with either WT-STAT3 or STAT3-d358L in the absence or presence of IL-6 stimulation (upper two panels). Expression and tyrosine phosphorylation of Flag-tagged WT STAT3 or STAT3-d358L (lower two panels) were also examined.

response to G-CSF stimulation via activating SHP-2/mitogen-activated protein kinase and JAK/STAT3 pathways (10). This mutant receptor, G133, is a chimeric receptor composed of the extracellular domain of the G-CSF receptor and the transmembrane and cytoplasmic domains of gp130 truncated 133 amino acids from the transmembrane domain. Mutation of the tyrosine residue in the YXXQ motif within G133 (G133F3) abolished STAT3 activation and, thus, cell proliferation driven by G-CSF (10). G133F3 cells were transduced with the pMX-puro vector carrying the WT STAT3, STAT3C, STAT3-d358L, a constitutively active mutant H-Ras (H-RasV12), or the expression vector alone (mock). Expression levels of WT STAT3, STAT3C, and STAT3-d358L were similar as judged by Western blotting (Fig. 7B, upper panel). The expression and activation of H-RasV12 were confirmed by Western blotting (Fig. 7B, lower panel, input lane) and by a pull-down assay using GST–Raf-RBD (Fig. 7B, lower panel, other lanes), respectively. As shown in Fig. 7A, STAT3-d358L but neither WT, STAT3C, H-RasV12, nor mock treatment promoted cell proliferation of G133F3 cells under G-CSF stimulation, suggesting

that the STAT3-d358L mutant is biologically functional and could be a useful tool to study the physiological roles of STAT3 activation. This result also indicates that STAT3-d358L is stronger than STAT3C in inducing STAT3-dependent cell growth, which is consistent with their transcriptional activities (Fig. 5B).

Interestingly, the tyrosine-phosphorylated form of STAT3-d358L accumulated to the nucleus after IL-6 stimulation more evidently than that of the WT STAT3 (Fig. 7C). Importantly, the STAT3-d358L bound MgcRacGAP and Rac1 more strongly than the WT in the absence or presence of IL-6 stimulation (Fig. 7D). Although most of the phosphorylated form of overexpressed WT STAT3 remained in the cytoplasm (Fig. 7C), this was probably because p-STAT3 requires MgcRacGAP/Rac1 as cofactors to enter the nucleus and these cofactors are limiting the nuclear translocation of p-STAT3. Taken together, our results strongly indicate that the interaction of STATs with MgcRacGAP accompanied by GTP-bound Rac1 plays critical roles in regulating STAT functions through facilitating both tyrosine phosphorylation of STATs and nuclear translocation of p-STATs.

DISCUSSION

We originally identified MgcRacGAP in a search for key molecules that are involved in the IL-6-induced macrophage differentiation of M1 cells (18) and found that MgcRacGAP and Rac1 form a ternary complex with STAT3 and are required for STAT3 activation (43). We also reported that MgcRacGAP localizes to the midbody of dividing cells and plays a crucial role in the completion of cytokinesis, thus playing a distinct role in the mitotic phase (12, 33). We recently found that GTP-bound Rac1 and MgcRacGAP are required for nuclear translocation of p-STATs via the importin pathway in an in vitro nuclear transport assay (17). In this paper, to identify the molecular mechanisms of how GTP-bound Rac1 and MgcRacGAP facilitate complex formation of p-STATs with importin αs, we used MgcRacGAP conditional knockout chicken DT40 cells (5C cells) as well as a nuclear transport assay and demonstrated that the NLS of MgcRacGAP plays a critical role in the nuclear translocation of p-STAT3/5. Although the biological functions of STAT3 and STAT5 are not identical, we demonstrated that nuclear import of p-STAT3 and p-STAT5 was mediated by MgcRaGAP and its NLS, and the molecular mechanisms are common.

Liu et al. (25) reported that constitutive nuclear import of STAT3 monomer is independent of tyrosine phosphorylation and is mediated by importin α3. They found that a deletion mutant of STAT3 (d150-163) (aa 150 to 162; DVRKRVQDL EQKM) did not enter the nucleus. However, the substitution mutant of the basic amino acid cluster in this sequence did not hamper nuclear accumulation. Based on these results, they reasoned that aa 150 to 162 play a role in a conformational structure that is required for nuclear import (25). Similarly, Zeng et al. reported that aa 138 to 165 of STAT5B are required for constitutive nuclear import of STAT5B monomer but that this region does not harbor polybasic amino acids (49). Thus, it was not clear whether STAT3 and STAT5 harbor a functional NLS or whether dimer formation creates a polybasic NLS of STAT3 and STAT5. We here propose that MgcRacGAP accompanied by GTP-bound Rac1 functions as an NLS-containing nuclear chaperone toward p-STATs (Fig. 2B and C). Interestingly, Rac1 was reported to play a role in the nuclear import of SmgGDS and p120 catenin (22), members of the importin α-like armadillo family of proteins (4, 38). The C-terminal region of Rac1, but not Rac2 or Rac3, contains a polybasic region, which may function as an NLS. However, Lanning et al. (22) also suggested that the interaction of Rac1 with its GTP exchange factor SmgGDS was qualitatively different from that of NLS-containing molecules with importin αs. Consistent with this, we failed to detect direct interactions of GTP-bound Rac1 with importin αs in either the in vitro binding assay or yeast two-hybrid assay (data not shown). Therefore, it is unlikely that GTP-bound Rac1 serves directly as an NLS-containing chaperone of p-STATs. The results shown in Fig. 2C strongly indicate that GTP-bound Rac1 activates the NLS MgcRacGAP associating with p-STATs; however, the precise molecular mechanism for the requirement of Rac1 remains to be clarified by structural analysis.

The present results demonstrate that the bipartite NLS (182KRR/199KK) of MgcRacGAP is essential for the nuclear transport and the transcriptional activation of p-STATs in living cells (Fig. 3G and H and 4A). The results of the nuclear-cytosol fractionation analysis using the 5C cells expressing 199AA and 182AAA/199AA (Fig. 3G) also suggested that the preferential nuclear localization of MgcRacGAP is mediated by the importin pathway in living cells. However, in the nuclear transport assay using semi-intact cells and purified proteins, nuclear translocation of MgcRacGAP was not achieved by the addition of importin α/β pathway proteins alone and, interestingly, further addition of p-STATs and GTP-bound Rac1 was required for nuclear translocation of MgcRacGAP (see Fig. S3A and B in the supplemental material). This raised a question of why overexpressed MgcRacGAP predominantly accumulated to the nucleus in HeLa cells, where STATs were not extensively activated. In addition, purified MgcRacGAP pulled down importin αs from the HeLa cell lysate (see Fig. S1B in the supplemental material), while it did not bind purified importin αs in the in vitro binding assay (Fig. 2C and data not shown). These results suggest that the NLS of MgcRacGAP can be activated by other cargo proteins as well as by p-STAT and GTP-bound Rac1. Thus, MgcRacGAP may function as a nuclear chaperone for not only p-STATs but also another nuclear protein(s).

The conditional knockout of MgcRacGAP in 5C cells decreased the G-CSF-induced tyrosine phosphorylation of STAT3 (Fig. 3C), and small interfering RNA-mediated MgcRacGAP knockdown in Ba/F3 cells also reduced tyrosine phosphorylation of STAT5 (17). These results implied that MgcRacGAP functions as an upstream regulator of STAT activation as well. In relation to this, STAT mutants harboring deletions in the βb-βc loop showed enhanced interaction with MgcRacGAP and became constitutively active (Fig. 5 and 6). It should be noted that the extent of tyrosine phosphorylation of STAT3-d358L without stimulation was weaker than that of WT 16 h after IL-6 stimulation (Fig. 7D), although the association of STAT3-d358L with MgcRacGAP/Rac1 was stronger than that of WT under the same conditions (Fig. 5C and 7D). These results indicate that the stronger association of the constitutively active STAT mutants with MgcRacGAP was not a

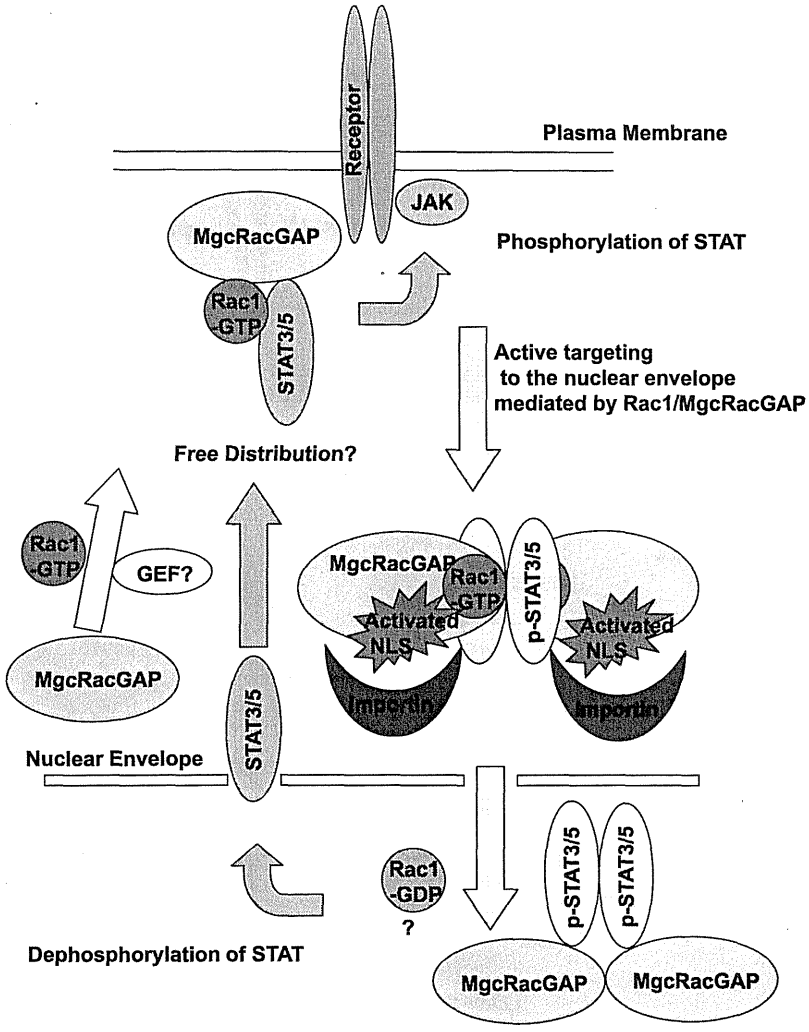

FIG. 8. A current model of nuclear import of p-STATs and a working hypothesis for membrane targeting and phosphorylation of STATs. In the present work, we demonstrated that the NLS of MgcRacGAP accompanied by GTP-bound Rac1 is essential for nuclear translocation of p-STATs via importin α/β. We also propose that binding of MgcRacGAP to STATs is required for their tyrosine phosphorylation after cytokine stimulation. Interestingly, the mutants that preferentially bind MgcRacGAP become constitutively active. Altogether, we conclude that MgcRacGAP critically functions both as a mediator of STAT's tyrosine phosphorylation and as an NLS-containing nuclear chaperone of p-STATs.

secondary result following the enhanced tyrosine phosphorylation of these mutants, and they imply a positive role for MgcRacGAP in facilitating STAT activation. In this context, it is interesting to note that V12Rac1 induced translocation of MgcRacGAP to the plasma membrane (see Fig. S5 in the supplemental material) and that MgcRacGAP bound JAK2 (17). In addition, the interaction of the STAT3-Y704F mutant, which does not undergo tyrosine phosphorylation, with MgcRacGAP was enhanced by IL-6 stimulation, similar to that of the WT STAT3 (data not shown). This indicates that the IL-6-induced MgcRacGAP interaction with STATs does not require tyrosine phosphorylation of STATs and occurs before their tyrosine phosphorylation. Based on these observations, we propose a model of STAT nucleo-cytoplasmic shuttling regulated by Rac1/MgcRacGAP (Fig. 8).

One important finding of the present paper is that the abilities of STAT mutants to bind MgcRacGAP correlated well with the activation of STATs (Fig. 5 and 6). To reveal the molecular mechanisms of MgcRacGAP-mediated regulation of STAT phosphorylation, we conducted an in vitro kinase reaction of purified STAT5 using purified JAK2 in the presence or absence of Rac1 and MgcRacGAP. However, STAT phosphorylation was not enhanced by the addition of Rac1/MgcRacGAP in this mixture (data not shown). Based on the result that MgcRacGAP binds JAK2, we speculate that MgcRacGAP regulates STAT phosphorylation by conveying STAT proteins to JAK2 or by serving as a scaffold for the interaction of JAK2 and STAT.

We also observed that STAT3-d358L bound MgcRacGAP more strongly than WT STAT3 did in yeast (data not shown). In the crystal structure of tyrosine-phosphorylated STAT3β (2) (PDB ID 1BG1), the MgcRacGAP binding DB2 region includes the C terminus of the βa′ strand, the DNA-bound βa′-βb loop, the βb strand, the βb-βc loop, and the N terminus